Arabian Journal of Geosciences (2019) 12: 380
https://doi.org/10.1007/s12517-019-4498-6

ORIGINAL PAPER

The depositional history of near-surface Qatar aquifer rocks and its impact on matrix flow and storage properties

John M. Rivers[1] · Sabrina L. Skeat[1] · Ruqaiya Yousif[1] · Chengjie Liu[2] · Elizabeth Stanmore[3] · Po Tai[2] · Sharifa M. Al-Marri[4]

Received: 11 December 2018 / Accepted: 23 April 2019 / Published online: 10 June 2019

Abstract

Carbonates and evaporites of Paleogene age form the shallow-aquifer rocks mantling most of Qatar, including the Paleocene and Lower Eocene Umm er Radhuma Formation and the Lower to Middle Eocene Rus and Dammam Formations. A core-based study was carried out to improve general understanding of the stratigraphic controls on aquifer matrix properties in Qatar. A cumulative total of 377 m of 10-cm-diameter core was recovered from three boreholes in central and northern Qatar, drilled to depths of greater than 120 m. Sedimentological attributes of these rocks were investigated through core and thin-section description, X-ray diffraction-based mineralogical assessment, as well as whole-rock stable isotopic analysis and integrated with interpretation of gamma-ray logs. Stratigraphic correlation of the penetrated intervals was then undertaken using sequence stratigraphic concepts and isotope stratigraphy ($\delta^{13}C$ trends) in the context of recently published regional paleomaps and structural studies. In the area of Qatar, the Umm er Radhuma Formation and the overlying Traina Member of the Rus Formation were deposited in marine settings of two different basins. These basins, which extended to the south and north of Qatar, respectively, are interpreted to have been separated by a topographic high, the location of which was controlled by the presence of high-angle normal faults. The southern basin was more restricted and was the site of extensive evaporite and clay-rich siliciclastic deposition during early stages of Rus Formation. Similar evaporites and fine siliciclastic deposits are not observed in time-equivalent strata of the northern basin. During subsequent deposition of the Al Khor Member of the Rus Formation, as well as the Dammam Formation, the basins appear to have been interconnected, and fine-grained siliciclastic deposits are interbedded with, but subordinate to, carbonate strata across Qatar. Most rocks recovered for this study are dolomitic, and dolomitic rocks free of other mineral phases tend to have significant porosity (20–50%) and permeability (10–1000 mD). Decreased connectivity, flow, and storage capacity are caused by (1) the presence of gypsum beds and nodules (only southern Qatar, upper Umm er Radhuma Formation, and Rus Formation), (2) the presence of pore-occluding clays (typically palygorskite) to varying degrees in all formations, and (3) the occurrence of diagenetic calcites, most commonly in the Dammam Formation. Aquifer quality of the near-surface rocks of Qatar is in large part a function of their depositional history and is to a degree predictable using reconstruction of basin architecture, as well as sequence stratigraphic concepts.

Keywords Qatar aquifer rocks · Matrix flow · Storage properties · Rus Formation · Dammam Formation · Umm Er Radhuma Formation

Editorial handling: Abdullah M. Al-Amri

Electronic supplementary material The online version of this article (https://doi.org/10.1007/s12517-019-4498-6) contains supplementary material, which is available to authorized users.

✉ John M. Rivers
John.m.rivers@exxonmobil.com

[1] Qatar Center for Coastal Research, ExxonMobil Research Qatar, Science and Technology Park, Tech2, PO Box 22500, Doha, Qatar

[2] ExxonMobil Exploration Company, Houston, TX, USA

[3] School of Earth Sciences, The University of Bristol, Beacon House, Queens Road, Bristol, UK

[4] Qatar Petroleum, Doha, Qatar

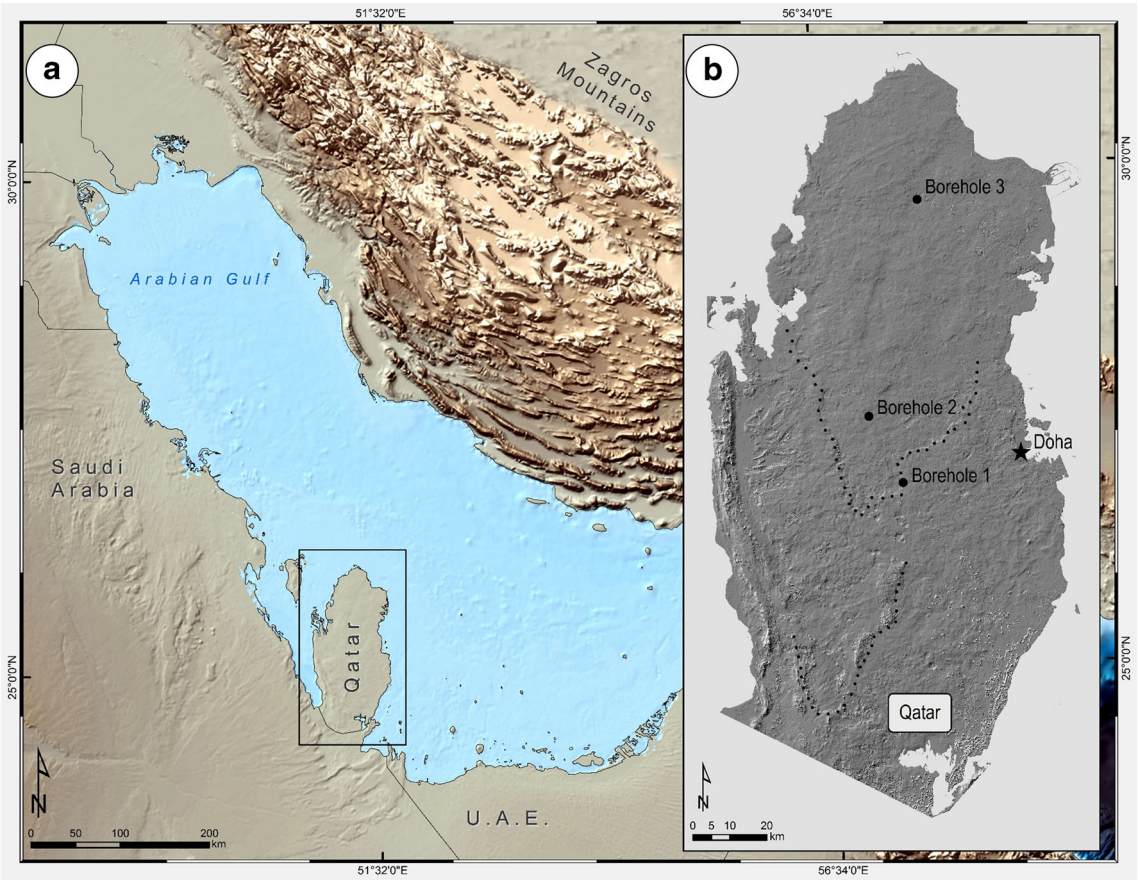

Fig. 1 **a** Regional map showing the location of Qatar (GEBCO_08 Grid, version 20100927). **b** Map of Qatar showing borehole locations as well as outlining a V-shaped surface escarpment in central Qatar and V-shaped outcrops of the Dam Formation in southwestern Qatar. (Satellite image and hillshade supplied and used by permission of the Qatar Center for Geographic Information Systems)

Introduction

The state of Qatar forms a peninsula protruding northward from Saudi Arabia into the Arabian Gulf, a shallow foreland basin of the Zagros Mountains (Fig. 1). The country is mantled by Cenozoic rocks (Cavelier et al. 1970; Seltrust Engineering Limited 1980) of mostly Eocene age (Rus and Dammam Formations), with the less extensive Miocene and Pliocene rocks of the Dam and Hofuf Formations outcropping only along fault-controlled jebels in southern Qatar (Figs. 2 and 3) (Rivers and Larson 2018). The subsurface Umm er Radhuma Formation (Paleocene-Eocene), which underlies the Rus Formation, does not outcrop in Qatar but is an important near-surface aquifer (Eccleston et al. 1981). Near the coast, the country is rimmed by Pleistocene and Holocene rocks and sediments reflective of its current arid setting, as a westward extension of the "Great Pearl Bank" (Purser 1973).

Studies of the Eocene rocks of Qatar are numerous and focus on hydrology (Eccleston et al. 1981; Baalousha 2016), diagenesis (Nasir et al. 2003; Holail et al. 2005), lithostratigraphy (Cavelier et al. 1970; Abu-Zeid and Boukhary 1984; Abu-Zeid 1991; Boukhary and Alsharhan 1998; Dill et al. 2003; Al-Saad 2005), biostratigraphy (Boukhary et al. 2011), and structure (Rivers and Larson 2018). Building on these studies, an effort was undertaken to update the understanding of the near-surface stratigraphy of Qatar in light of both the Rivers and Larson (2018) structural study, as well as recently published regional maps of Eocene depositional environments (Tai et al. 2016). Rock cores were recovered from boreholes that penetrated the upper ~ 120 m at three locations in central and northern Qatar (Fig. 1). Detailed rock textural classification and fossil identification, as well as measurements of mineralogical composition by X-ray diffraction (XRD), were carried out on these cores. These datasets were used for classification of depositional facies, as well as lithostratigraphic interpretation. Rocks from the three boreholes were then correlated using gamma-ray (GR) logs and bulk stable isotopic measurements, as well as sequence stratigraphic concepts. Trends in measured rock porosity and rock permeability (a property necessary for determining hydrologic conductivity) were also assessed in light of core location, lithostratigraphic designation, and mineralogical makeup. The purpose of this study was to improve the general understanding of Qatar aquifer rocks and the depositional controls on aquifer quality with respect to rock matrix flow and storage capacity.

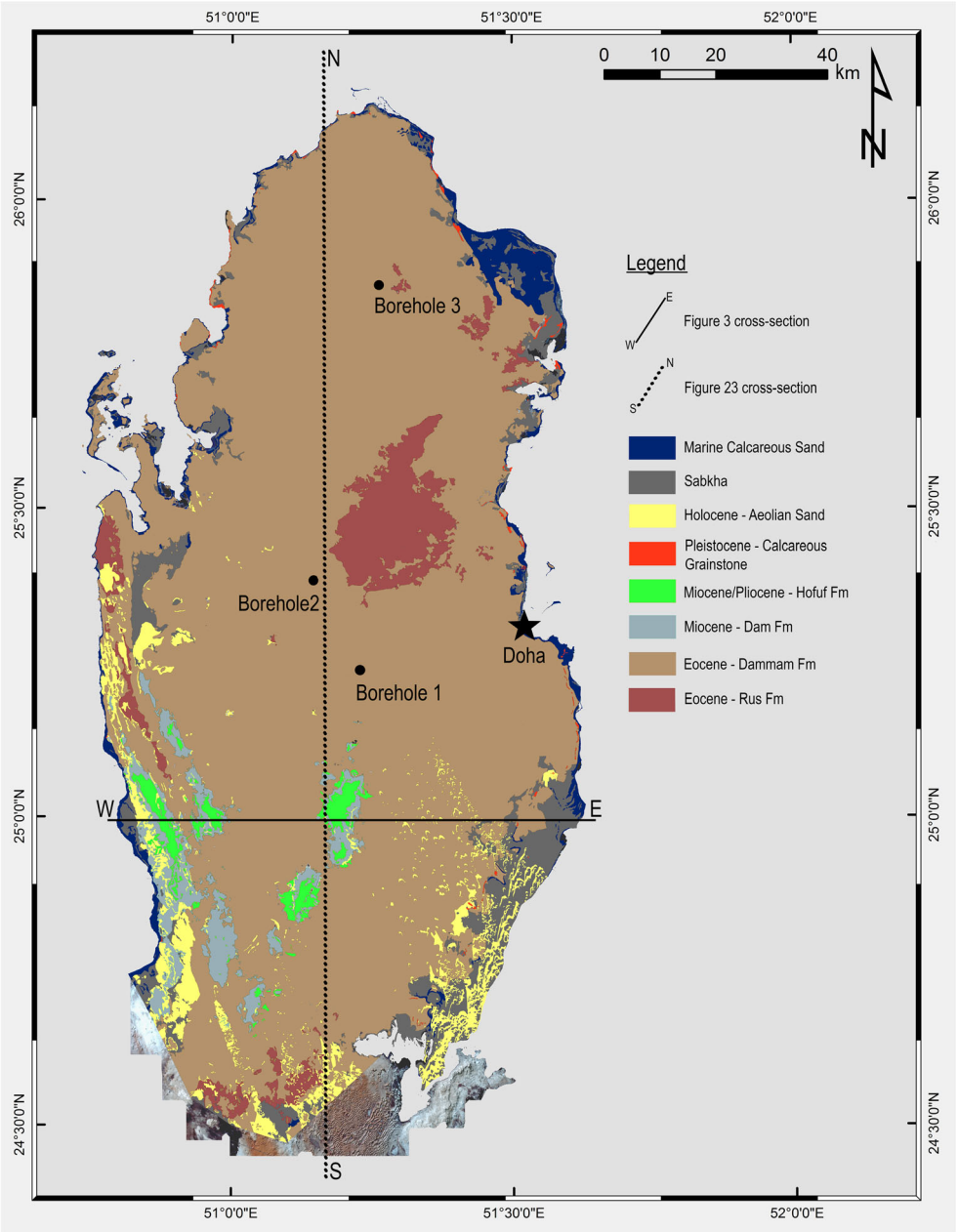

Fig. 2 Surficial geological map of Qatar after Cavelier (1970) and Seltrust Engineering (1985). Line of section is shown for Fig. 4 (E-W) and Fig. 23 (N-S)

Lithostratigraphic division

Based on published studies, the Paleogene rocks that comprise the near-surface aquifers of Qatar consist of three formations: (1) the Paleocene-Lower Eocene (Ypresian) Umm er Radhuma Formation, (2) the Lower Eocene (Ypresian) Rus Formation, and (3) the Middle Eocene (Lutetian/Bartonian) Dammam Formation (Cavelier et al. 1970; Cavalier 1975; Eccleston et al. 1981; Boukhary and Alsharhan 1998; Al-Saad 2005; Boukhary et al. 2011) (Figs. 2, 3, and 4). These formations are generally flat-lying and locally dissected by high-angle normal faults (Rivers and Larson 2018) (Fig. 3).

The Umm er Radhuma Formation does not outcrop in Qatar but is an important aquifer with a thickness between 100 and 370 m (Eccleston et al. 1981; Boukhary et al. 2011). Published lithological descriptions based on cuttings from Qatar boreholes show that the formation consists of off-white dolomitic limestones underlain by harder vesicular dolomite (Eccleston et al. 1981). Boukhary et al. (2011) studied foraminifera assemblages of the Umm er Radhuma Formation from the Dukhan field (western Qatar), where the formation thins to ~130 m. They divided the formation into three members (A, B, C) and showed that the Umm er Radhuma Formation yields a diverse assemblage of both planktonic and large benthic foraminifera,

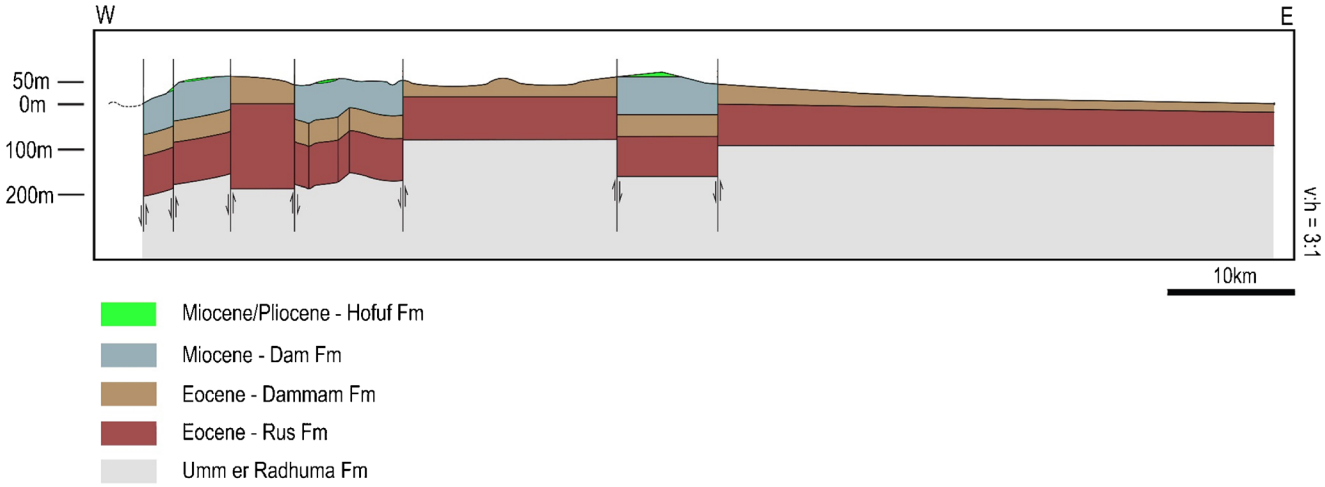

Fig. 3 East-west geologic cross section of Qatar near-surface rocks (line location in Fig. 2) after Rivers and Larson (2018)

reflecting open marine to sheltered lagoon depositional environments.

Overlying the Umm er Radhuma Formation is the Rus Formation, which is understood to vary in thickness across onshore Qatar between a minimum of 15 m in the Dukhan area to a maximum of 122 m in southwestern Qatar (Eccleston et al. 1981). The Rus Formation is generally considered to have been deposited in shallower marine environments relative to the Umm er Radhuma Formation (Eccleston et al. 1981). The depositional facies of the Rus Formation varies from north to south across Qatar, being segregated by a V-shaped escarpment apparent in satellite imagery (Fig. 1) (Eccleston et al. 1981; Abu-Zeid 1991; Al-Saad 2003). South of this escarpment, the Rus Formation consists of meter-scale dolomite-gypsum-clay cycles (Traina Member) interpreted to represent restricted lagoon to supratidal settings (Abu-Zeid 1991; Al-Saad 2003). This passes upwards into chalky dolomites and limestones with minor gypsum, marl, and clay intercalations (Al Khor Member) interpreted to have formed in more open marine settings (Al-Saad 2003). To the north of the escarpment, the thick gypsum and clay beds of the Traina Member are absent, and dolomitic limestone predominates, reflecting normal marine depositional conditions (Abu-Zeid 1991).

The Dammam Formation outcrops across much of Qatar and in northern Qatar varies in thickness between absence on the Qatar arch (central Qatar) (Fig. 2) and ~ 40 m along the western coast (Abu-Zeid 1991). The formation has been divided into five members (Cavelier et al. 1970; Cavalier 1975; Al-Saad 2005) including (1) the Rujm Aid Member (fossiliferous limestone, formerly the Fhaihil Velates Member), (2) the Midra Shale Member (argillaceous limestone), (3) the Alveolina Member (formerly the Dukhan Member, fossiliferous limestone with conspicuous *Alveolina* foraminifera, (4) the Umm Bab Member (marly dolomitic limestone), and (5) the Abaruq Member (dolomitic limestone). Commonly, not all members are present at one location. For example, in north-central Qatar, Al-Saad (2005) interprets the Dammam Formation to include the Midra Shale, Alveolina, and Umm Bab Members (well B, their Fig. 2), whereas Abu-Zeid (1991) interprets cores from the same area to only include Umm Bab Member (wells p35 and p27, their Fig. 2). In general, relative to the underlying Rus Formation, the Dammam Formation is interpreted to represent a return to more open marine conditions (Eccleston et al. 1981; Al-Saad 2005).

Methodology

Rock cores (10-cm-diameter) were recovered from boreholes located in central Qatar (borehole 1 to a depth of 134 m and borehole 2 to a depth of 120 m) and northern Qatar (borehole 3 to a depth of 123 m) (Fig. 1). Core recovery at all locations was > 95% of rocks penetrated, but cores from boreholes 2 and 3, both taken from within interpreted karst depressions (dolines), suffered from poor rock competency in several intervals. Cores from competent intervals were split and 5-cm plugs extracted at ~ 0.75 m intervals. The plugs were then measured for helium porosity and Klinkenberg permeability ($n = 317$) (Appendix 1), and a subset of these plugs were used for both bulk-mineral and clay-mineral identification by XRD ($n = 268$). Powders taken from selected core plugs were analyzed using standard powder XRD techniques. Mineral percentages for each sample were quantified using a proprietary approach at Core Laboratories. In all holes, gamma-ray geophysical logs were run after core recovery.

The split cores and thin-sections were described using Dunham's texture scheme (Dunham 1962), and fossil assemblages, as well as sedimentary structures, were interpreted (Table 1). Carbonate-rich samples were selected from the core for carbon and oxygen stable isotopic analyses ($n = 542$) (Appendix 2). Isotope measurements were performed at the Center for Stable Isotope Biogeochemistry (CSIB), University of California, Berkeley. Measurements were run on 10 to 100 μg sample weights of carbonate. Several replicates of one

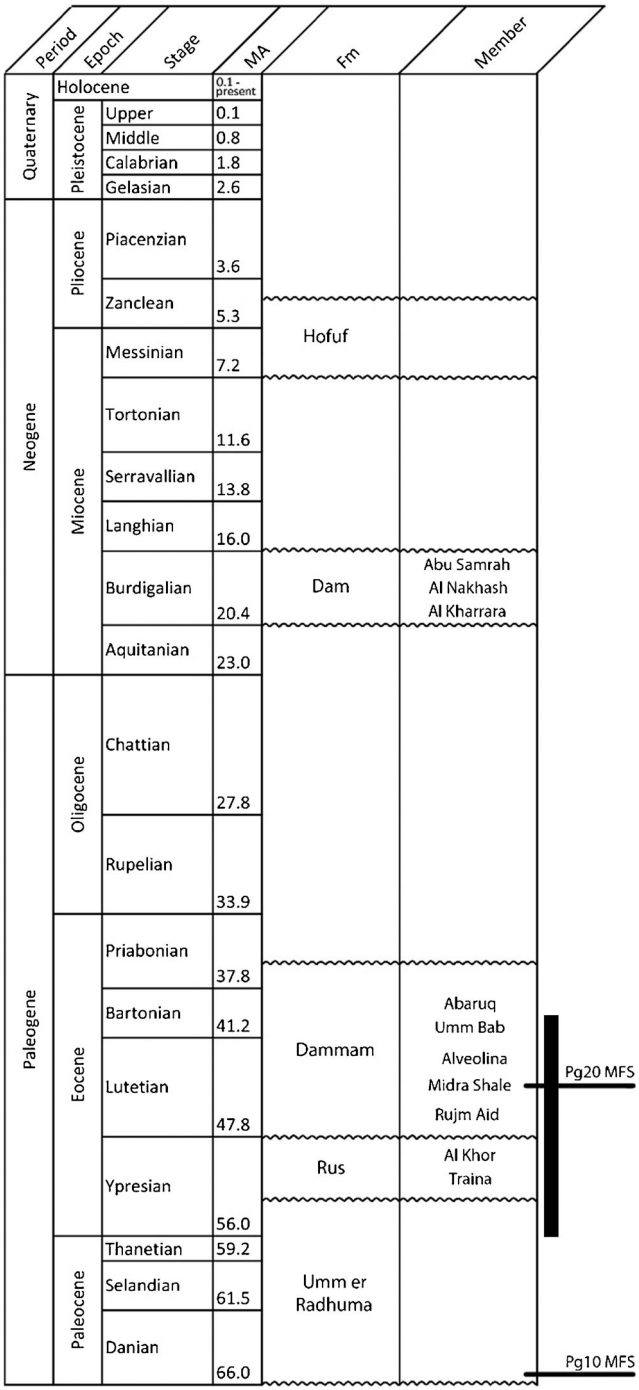

Fig. 4 Stratigraphic column for the near-surface rocks of Qatar (Cavelier, 1970, Boukhary and Alsharhan 1998; Al Saad and Ibrahim, 2002; Al-Saad 2005). Stratigraphic interval studied for this report is indicated by the vertical black bar on the right. Stratigraphic position of Arabian Plate maximum flooding surfaces Pg10 and Pg20 of Sharland et al. (2001) shown on the right

international standard (NBS19) and two lab standards were measured with each run. The overall external analytical precision is about ± 0.05‰ for $\delta^{13}C$ and about ± 0.07‰ for $\delta^{18}O$. Carbon and oxygen isotope compositions are reported in standard δ notation ($\delta^{13}C$ and $\delta^{18}O$) in units of per mil relative to Vienna Peedee Belemnite (VPDB) standard. $\delta^{18}O$ measurements for silicates were run at Queen's University Facility for Isotope Research.

Results

Lithological description

Integrated descriptions (textures, fossils, and dolomite crystal size) for cores from boreholes 1–3 are shown in Figs. 5, 6, and 7, respectively, with accompanying whole-rock-isotope and mineralogical data. Fossils could only be identified in dolomitized rocks where crystal sizes were small (< 20 μm) and where dolomite textures mimicked that of the original limestone. "Non-mimetic" dolomitic rock is of a type too coarse to discern original allochem structures. Plug porosity and permeability data are also displayed with depth, as is the gamma-ray well log. Based on mineralogy, textures, allochems, and sedimentary structures, the rocks from each borehole can be subdivided into several depth-delineated units of similar character. Table 1 reviews the attributes of each unit.

Borehole 1

Depth interval 134–69.8 m below surface Rocks consist of light- to dark-brown fining-upward cycles of variable thickness (Fig. 8a). Cycle bases are thick (meter-scale) dolomitic mud-lean packstones with a mottled appearance (Fig. 8a-1), interpreted to be the result of the mixing of mud-bearing and mud-free sediment by the action of burrowing organisms. In some instances, the cycle bases are floored by what appears to have been a coarse lag deposit (Fig. 8a-3). Cycles caps are centi- to decimeter-scale thin-bedded or laminated dolomitic wackestones or mudstones (Fig. 8a-2). The dolomite in cycle caps is finely-crystalline, and commonly, palygorskite clay is observed as a secondary mineral (Fig. 8b). Cycle bases are more coarsely crystalline and clay-free (Fig. 8c).

The presence of replacive (and minor displacive) gypsum nodules (Fig. 8d), ranging from millimeter-scale to the width of the core increases upwards from absence below 96.0 m below surface (mbs) to abundant near the top of the interval. Generally, identifiable allochems were obliterated in this interval by dolomitization, but dasyclad green algae and large benthic foraminifera can uncommonly be observed in thin section. In one ~ 20-cm-thick silicified interval at 127.0 mbs, fossils are better preserved (Fig. 9a–d). Identifiable allochems include large benthic foraminifers, most commonly *Nummulites* but also *Lockhartia* sp.,

Table 1 Summary of depositional textures, depositional structures, and grain types by borehole and depth interval

Borehole	Depth (mbs)	Lithology	Common textures	Common structures	Typical cycle	Large benthic Foraminifera	Small benthic Foraminifera	Planktonic Foraminifera	Molluscs	Other allochems
1	14.8–0	Calcite, palygorskite (karst infill), minor dolomite	Packstones and wackestones	Brecciation (karst)	Cyclicity not apparent—rocks karstified and becciated	*Nummulites* sp., *Lockhartia* sp., *Rotalia trochidiformis* sp., *Heterostegina* sp., *Daviesina* sp., *Opersulinasp* sp., *Alveolina* sp., *Eorupertia* sp., *Linderina* sp., *Coskinolina* sp., *Pseudolituonella* sp., *Orbitolites* sp., *Nummulites* sp., *Lockhartia* sp., *Rotalia trochidiformis* sp., *Heterostegina* sp., *Daviesina* sp., *Opersulinasp* sp., *Alveolina* sp., *Eorupertia* sp., *Linderina* sp., *Coskinolina* sp., *Pseudolituonella* sp., *Orbitolites* sp.	Miliolid	*Morozovella, Acarinina*	Small bivalves	Echinoid spines, sponge spicules, dasyclad green algae, rare corals, red algae
1	29.4.0–14.6	Calcite, dolomite, bedded palygorskite, bedded illite	Crystalline limestones, packstones, wackestones, clastic mudstones	Roots, minor laminations in fine clay-rich dolostones (algal mats), rip-up-clast--breccia	No consistent cyclicity	Absent	Miliolid, *Rotalia* sp., *Clavulina* sp., Miliolid, *Rotalia* sp., *Clavulina* sp.	Absent	Small bivalves, ostracods	Dasyclad green algae
1	61.3–29.4	Dolomite, bedded gypsum, bedded palygorskite	Packstones and wackestones, crystalline gypsum, clastic mudstone	Minor lamination in dolomite, roots in palygorskite, erosive surfaces above palygorskite beds	(1) Fine mimetic dolomite (base), (2) bedded gypsum, (3) palygorskite-rich clay (cap)	Absent	Miliolid, *Rotalia* sp., *Clavulina* sp., Miliolid, *Rotalia* sp., *Clavulina* sp.	Absent	Small bivalves, ostracods	Dasyclad green algae
1	69.8–61.3	Dolomite with abundant gypsum nodules, minor palygorskite	Packstones and wackestones, minor breccia	Straight and wavy lamination (algal mats), brecciated surfaces	Cyclicity not apparent—disrupted by gypsum replacement	*Coskinolina* sp., *Coskinolina* sp.	Miliolid, *Rotalia* sp., *Bolivina* sp., *Praerhapydionina* sp., Miliolid, *Rotalia* sp., *Bolivina* sp., *Praerhapydionina* sp.	Absent	Small bivalves, ostracods	Absent
1	134–69.8	Dolomite, gypsum nodules absent at base to common at top,	Mud-lean packstones grading to wackestones	Bioturbation, lamination	(1) Course lag (base), (2) bioturbated mud-lean dolo-packstones, (3) laminated palygorskite-rich fine dolo	*Nummulites*, *Lockhartia* sp., *Opertorbitolites* sp., *Miscellanea* sp., *Alveolina* sp., *Cribrobulimina* sp., *Pseudolituonella* sp., *Cymopolia kurdistanensis, Nummulites*, *Lockhartia*	Poor fossil ID due to obliterative dolomitization	Poor fossil ID due to obliterative dolomitization	Poor fossil ID due to obliterative dolomitization	Echinoid spines, sponge spicules, dasyclad green algae

Table 1 (continued)

Borehole	Depth (mbs)	Lithology	Common textures	Common structures	Typical cycle	Large benthic Foraminifera	Small benthic Foraminifera	Planktonic Foraminifera	Molluscs	Other allochems
		minor palygorskite			packstones/-wackestone (cap)	sp., *Opertorbitolites* sp., *Miscellanea* sp., *Alveolina* sp., *Cribrobulimina* sp., *Pseudolituonella* sp., *Cymopolia kurdistanensis*				
2	14.6–0	Calcite, palygorskite (karst infill), minor dolomite	Packstones and wackestones	Brecciation (karst)	Cyclicity not apparent—rocks karstified and becciated	*Nummulites* sp., *Alveolina* sp., *Lockhartia* sp., *Linderina* sp., *Coskinolina* sp., *Nummulites* sp., *Alveolina* sp., *Lockhartia* sp., *Linderina* sp., *Coskinolina* sp.	Miliolid, textularid, Rotalid	Absent	Small bivalves and gastropods	Echinoid Spines, dasyclad green algae
2	39.5–14.6	Dolomite, calcite, and palygorskite	Mudstone, wackestones, and packstones	Laminations, stromatolites, root traces, breccias (rip ups), and disturbed bedding	Absent	Absent	Miliolid	Absent	Absent	Mud rip-ups
2	62.4–39.0	Dolomite and minor chalcedony	Wackestones	Bioturbation, minor lamination	Not apparent	Poor fossil ID due to obliterative dolomitization	Poor fossil ID due to obliterative dolomitization	Poor fossil ID due to obliterative dolomitization	Poor fossil ID due to obliterative dolomitization	Poor fossil ID due to obliterative dolomitization
2	73.2–62.4	Dolomite and minor calcite	Wackestones	Roots/exposure diagenesis	Not apparent	Poor fossil ID due to obliterative dolomitization	Poor fossil ID due to obliterative dolomitization	Poor fossil ID due to obliterative dolomitization	Poor fossil ID due to obliterative dolomitization	Poor fossil ID due to obliterative dolomitization
2	105.4–73.2	Dolomite	Packstones and wackestones/-dolomite silt	Bioturbation, lamination	Cyclicity not apparent—rocks karstified and becciated	Poor fossil ID due to obliterative dolomitization	Poor fossil ID due to obliterative dolomitization	Poor fossil ID due to obliterative dolomitization	Molds apparent	Poor fossil ID due to obliterative dolomitization
2	120–105.4	Dolomite	Packstones and wackestones	Bioturbation, lamination	Cyclicity not apparent—rocks karstified and brecciated	Poor fossil ID due to obliterative dolomitization	Poor fossil ID due to obliterative dolomitization	Poor fossil ID due to obliterative dolomitization	Poor fossil ID due to obliterative dolomitization	Poor fossil ID due to obliterative dolomitization
3	7.7–0	Dolomite and calcite	Crystalline dolostones, crystalline limestones	Karst brecciation	Not apparent	*Nummulites* sp., *Alveolina* sp., *Nummulites* sp., *Alveolina* sp.	Miliolid?	Poor fossil ID due to obliterative dolomitization and karst	Small bivalves, gastropods	Rare Dasyclad Green Algae
3	26.5–7.7	Dolomite, bedded palygorskite, calcite	Packstones, wackestones, mudstones, clastic mudstones, crystalline limestones	Bioturbation, lamination	(1) Bioturbated dolomitic rocks, (2) laminated dolomitic rocks, (3) laminated palygorskite	Absent	Miliolid, *Rotalia* sp., textularids, Miliolid, *Rotalia* sp., textularids	Absent	Minor bivalves and gastropods	Rare Dasyclad Green Algae
3	60.2–26.5	Dolomite			Not apparent	Rare *Nummulities* sp.				

Table 1 (continued)

Borehole	Depth (mbs)	Lithology	Common textures	Common structures	Typical cycle	Large benthic Foraminifera	Small benthic Foraminifera	Planktonic Foraminifera	Molluscs	Other allochems
			Mud-lean packstones, packstones, wackestones, grainstones	Bioturbation, lamination, ripples?		Generally poor fossil ID due to obliterative dolomitization Rare *Nummulities* sp. Generally poor fossil ID due to obliterative dolomitization	Miliolid, *Rotalia* sp., Miliolid, *Rotalia* sp.	Poor fossil ID due to obliterative dolomitization	Rare small bivalve and gastropod apparent	Rare Dasyclad Green Algae
3	68.2–60.2	Dolomite, minor calcite	Mud-lean packstones	Bioturbation	Not apparent	Poor fossil ID due to obliterative dolomitization	Miliolid?	Poor fossil ID due to obliterative dolomitization	Rare small bivalve and gastropod apparent	Rare Dasyclad Green Algae
3	99.7–68.2	Dolomite, minor calcite near top	Mud-lean packstones, packstones, wackestones? Dolomite silt	Bioturbation	Cyclicity not apparent—rocks karstified and becciated	Molds? Poor fossil ID due to obliterative dolomitization	Poor fossil ID due to obliterative dolomitization	Poor fossil ID due to obliterative dolomitization	Molds? Poor fossil ID due to obliterative dolomitization	Rare dasyclad Green Algae
3	122.2–99.7	Dolomite	Mud-lean packstones, packstones, wackestones	Bioturbation	Course bioturbated mud-lean packstone capped by thin packstone or wackestone	Absent	Miliolid, *Rotalia* sp.	*Subbotina* sp.? *Parasubbotina* sp.?	Abundant large bivalves and gastropods	Dasyclad Green Algae

Opertorbitolites sp., *Miscellanea* sp., *Alveolina* sp., *Cribrobulimina* sp., and *Pseudolituonella* sp. Small benthic foraminifers (miliolid and textularid types), dasyclad green algae (*Cymopolia kurdistanensis* sp.), as well as echinoid spines and plates, sponge spicules, and dasyclad algae are also observed (Table 1).

Depth interval 69.8–61.3 mbs Rocks are off-white (Fig. 10), a significantly lighter hue than those below. Cyclicity is difficult to identify largely due to disturbance by intense gypsum-nodule-growth. Pervasive dolomitization is, in part, mimetic so that textures are more easily interpreted and allochems identifiable. Textures appear to fine upward from packstones between 70.0 and 66. mbs, to wackestones between 66.0 and 61.0 mbs (Fig. 5). These rocks are commonly laminated, and both straight and crinkled laminations are observed (Fig. 10a). Allochems consist of small benthic foraminifers, including miliolids, *Rotalia* sp., *Bolivina* sp., *Praerhapydionina* sp., and *Coskinolina* sp., as well as small bivalves and ostracods (Fig. 10b). The interval is capped by a breccia at 61.3 mbs overlain by a sharp erosion surface that cross-cuts the breccia (Fig. 10c).

Depth interval 61.3–29.4 mbs Meter-scale cycles are apparent, with bases composed of off-white finely crystalline mimetic dolomite, overlain by bedded gypsum, and capped by green palygorskite clay beds (Fig. 11a). Skeletal grains apparent in the dolomitized sections are similar to those of the underlying interval, including the small benthic foraminifera *Rotalia* sp., and as *Clavulina* sp., as well as miliolid types. Ostracods and echinoderm plates are also observed. High-abundance, low-diversity assemblages are noted, including miliolid dolo-grainstones (as intraclasts) (Fig. 11b). In some parts of this interval, gypsum is interbedded with stingers of dolomite mudstone. More commonly, gypsum deposits are several meters thick, display radiating crystals (Fig. 11c), and infrequently include anhydritic layers. Some palygorskite beds include root traces, and capping surfaces are commonly erosional or bored. The top of this interval consists of a ~3-m-thick clay deposit that alternates between green (palygorskite-rich) and red/brown (illite-rich) beds, with crinkly lamination observed in thin section (Fig. 11d).

Depth interval 29.4–14.6 mbs Decimeter- to meter-thick coarsely crystalline vuggy cream- to gray-colored calcite beds are prominent, particularly below 22.4 mbs, and found in association with thin, root-trace-bearing palygorskite and illite clay deposits (Fig. 12a). Microcodium textures are commonly observed in thin sections of the crystalline limestone beds (Fig. 12b). Above 22.4 mbs, rocks return to white dolomitic mudstones, wackestones, and packstones rich in peloids, small benthic foraminifers (miliolids), and small molluscs. At the top of the interval, a coarsely crystalline limestone is observed with a thin cap of clay-rich rock-bearing root traces.

Depth interval 14.6–0 mbs With the exception of a thin interval of clay-rich dolomitic rock between 13.7 and 12.6, these rocks are composed of cream-colored and Fe-oxide-stained lime wackestones and packstones, with rare intervals of coarse crystalline limestone. The skeletal assemblage is diverse (Fig. 12c), including large benthic foraminifers (*Rotalia trochidiformis* sp., *Heterostegina* sp., *Nummulites* sp., *Daviesina* sp., *Opersulina* sp., *Alveolina* sp., *Eorupertia* sp., *Linderina* sp., *Coskinolina* sp., *Pseudolituonella* sp., *Orbitolites* sp.), small miliolids, planktonic foraminifers, as well as small molluscs, echinoid spines, dasyclad green algae, and other more minor constituents (Table 1). Centimeter-scale concretions are observed in the limestones of this interval (Fig. 12d). Particularly above 7.5 mbs, the rocks are brecciated and karstified.

Borehole 2

Depth interval 120–105.4 mbs This interval includes very dark-grey, light-grey, or brown bioturbated dolo-packstones and mud-lean packstones. Almost all dolomite is obliterative, but where allochems ghosts are identifiable, they include large benthic (*Nummulites* sp.) foraminifers (Fig. 13a) as well as dasyclad green algae, echinoderm fragments, and molluscs. Rocks were largely broken and disturbed during recovery masking possible cyclicity. The interval is capped by a thin breccia with associated diffuse silica cements directly below (Fig. 13b).

Depth interval 105.4–73.2 mbs This interval includes both rocks and sediments. Sediments are poorly-sorted sands composed of crystalline dolomite grains, with dolomitic clasts (up to cobble size) in float (Fig. 13c). Decimeter-thick layers of dolomitic rocks are observed within the succession of dolomitic sediment, some of which display horizontal lamination indicating they are not rotated (Fig. 13d). Rock-dominated intervals are meter-scale dolomitic light- to dark-brown mottled packstones, commonly interpreted as mud-lean, with prominent burrow structures that are intercalated with centimeter-scale laminated or burrowed wackestones and mudstones. Dolomitization is mostly obliterative, masking the original fossil assemblage. Bivalve molds and sparse large benthic-foraminifers and dasyclad green-algae ghosts

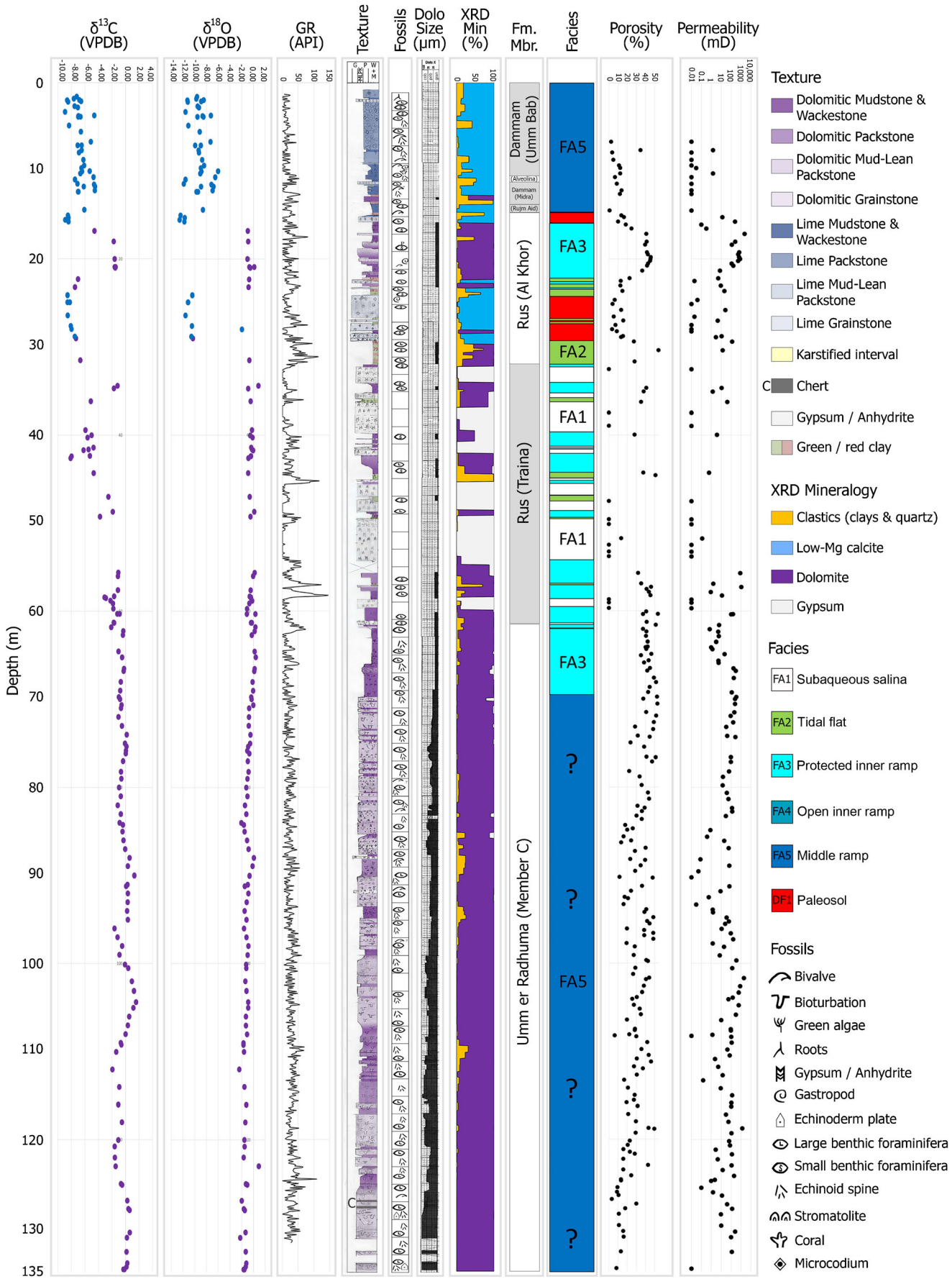
δ13C (VPDB)
δ18O (VPDB)
GR (API)
Texture
Fossils
Dolo Size (µm)
XRD Min (%)
Fm. Mbr.
Facies
Porosity (%)
Permeability (mD)
Depth (m)
Dammam (Umm Bab)
Rus (Al Khor)
Rus (Traina)
Umm er Radhuma (Member C)
FA5
FA3
FA2
FA1
FA1
FA3
?
?
FA5
?
?
Texture
Dolomitic Mudstone & Wackestone
Dolomitic Packstone
Dolomitic Mud-Lean Packstone
Dolomitic Grainstone
Lime Mudstone & Wackestone
Lime Packstone
Lime Mud-Lean Packstone
Lime Grainstone
Karstified interval
Chert
Gypsum / Anhydrite
Green / red clay
XRD Mineralogy
Clastics (clays & quartz)
Low-Mg calcite
Dolomite
Gypsum
Facies
FA1 Subaqueous salina
FA2 Tidal flat
FA3 Protected inner ramp
FA4 Open inner ramp
FA5 Middle ramp
DF1 Paleosol
Fossils
Bivalve
Bioturbation
Green algae
Roots
Gypsum / Anhydrite
Gastropod
Echinoderm plate
Large benthic foraminifera
Small benthic foraminifera
Echinoid spine
Stromatolite
Coral
Microcodium

◀ **Fig. 5** Borehole 1 core description integrating whole-rock stable isotope composition ($\delta^{18}O$ and $\delta^{13}C$), down-hole gamma-ray (GR), rock texture, fossil assemblage, dolomite crystal size, XRD-based mineralogical composition, formation, and member boundary interpretation, depositional facies interpretation, as well as plug porosity and permeability measurements

were tentatively identified. Notably, a 3-cm-thick chert bed is conspicuous at a depth of 88.3 mbs (Fig. 13e). In the upper ~10 m of the interval, centimeter-thick concentrations of disseminated calcite crystals are irregularly observed in the dolomitic rocks.

Depth interval 73.2–62.4 mbs Similar to the interval immediately below (*105.4–73.2 mbs*), both dolomitic sediments and rocks are observed in this interval. The sediment is mostly composed of fine sand-sized crystalline dolomite grains. Lithified intervals are interpreted as dolomitic wackestones and mudstones that in some cases appear to have been brecciated by synsedimentary reworking. Allochem ghosts are rare, mostly dasyclad green algae. A marked difference in this interval relative to the underlying interval is that the rocks and sediments are lighter in color (a lighter hue of brown). Course crystalline calcite becomes an important phase toward the top of the interval, which is marked by a brecciated and fractured surface (Fig. 14a).

Depth interval 62.4–39.0 mbs Deposits are off-white, mostly-pure dolomite with minor disseminated chert and calcite crystals. Between 62.4 and 46.0 mbs, fine sands composed of dolomite crystals are interbedded with rubble comprised of dolomitic rocks. Intact mudstones intercalated with centimeter-thick wackestones or packstones are observed above this depth. Rocks display burrows with coarsely dolomitized fill in these overall finely-crystallized deposits. These are interpreted to represent grain-filled burrows in mud-dominated sediment (Fig. 14b). Other sedimentary structures are mostly absent, and allochem ghosts are limited to a rare dasyclad green algae in these obliteratively-dolomitized deposits.

Depth interval 39.0–14.6 mbs Off-white dolomitic mudstones, wackestones, and packstones are observed to be intercalated with decimeter-thick beds of palygorskite clay and intermittent crystalline limestone. Dolomitic rocks are variably bioturbated or laminated and, along with palygorskite beds, appear to have been disturbed by synsedimentary reworking and brecciation (Fig. 14c). Mud cracks are also interpreted in this interval (Fig. 14d). Dolomite remains largely obliterative, but miliolid foraminifers are observed in some thin sections.

Depth interval 14.6–0 mbs This interval includes highly karstified and recrystallized limestones with minor dolomitic intervals. Dolomitic intervals are associated with centimeter-thick layers of palygorskite, and ghosts of allochems are not apparent. *Nummulites*-rich packstone is observed between 13.5 and 12.0 mbs. Limestones between 12.0 and 8.0 mbs are mostly non-mimetically recrystallized and bear large vugs filled with white palygorskite clay (Fig. 14e). Limestones above 8.0 mbs show a more diverse assemblage including the large benthic foraminifers *Nummulites*, *Alveolina* sp., *Lockhartia* sp., *Linderina* sp., and *Coskinolina* sp. Other allochems include small benthic foraminifers, small bivalves, gastropods, echinoid spines, and dasyclad green algae.

Borehole 3

Depth interval 122.2–99.7 mbs Rocks are light- to dark-gray or light-brown meter-scale beds of bioturbated dolomitic mud-lean packstones typically capped by centimeter-thick dolomitic packstones and wackestones. Mollusc molds are apparent in some sections of core (Fig. 15a). In thin section, dolomite is commonly obliterative, but where allochems are identifiable, they include molluscs, as well as small benthic and planktonic foraminifers, and dasyclad green algae (Fig. 15b, c). The top of the interval is represented by a conspicuous 20-cm-thick, black, brecciated dolomitic rock.

Depth interval 99.7–60.2 mbs Light-brown dolomitic rocks and sediments typify this interval. The dolomite below 90.6 mbs is lithified, displays evidence of bioturbation from the precursor limestone, and is tentatively interpreted as mud-lean packstone. Much of the recovered rock in this interval was poorly lithified. Between 90.6 and 74.2, fine sand and silt composed of dolomite crystals were recovered (Fig. 15d). Undisturbed rocks are again observed above this interval and consist mostly of bioturbated dolomitic packstones and wackestones. Notably a 10-cm-thick band of silicified rock is observed at 71.35. Sparse ghosts of dasyclad green algae are apparent in thin section, and rare molds of large benthic foraminifers and bivalves have been tentatively identified (Fig. 15e). The uppermost 10 m of the interval includes sparse centimeter-scale beds of crystalline calcite. Palygorskite clay is a common secondary mineral. The interval is capped by a 2-cm-thick palygorskite clay deposit.

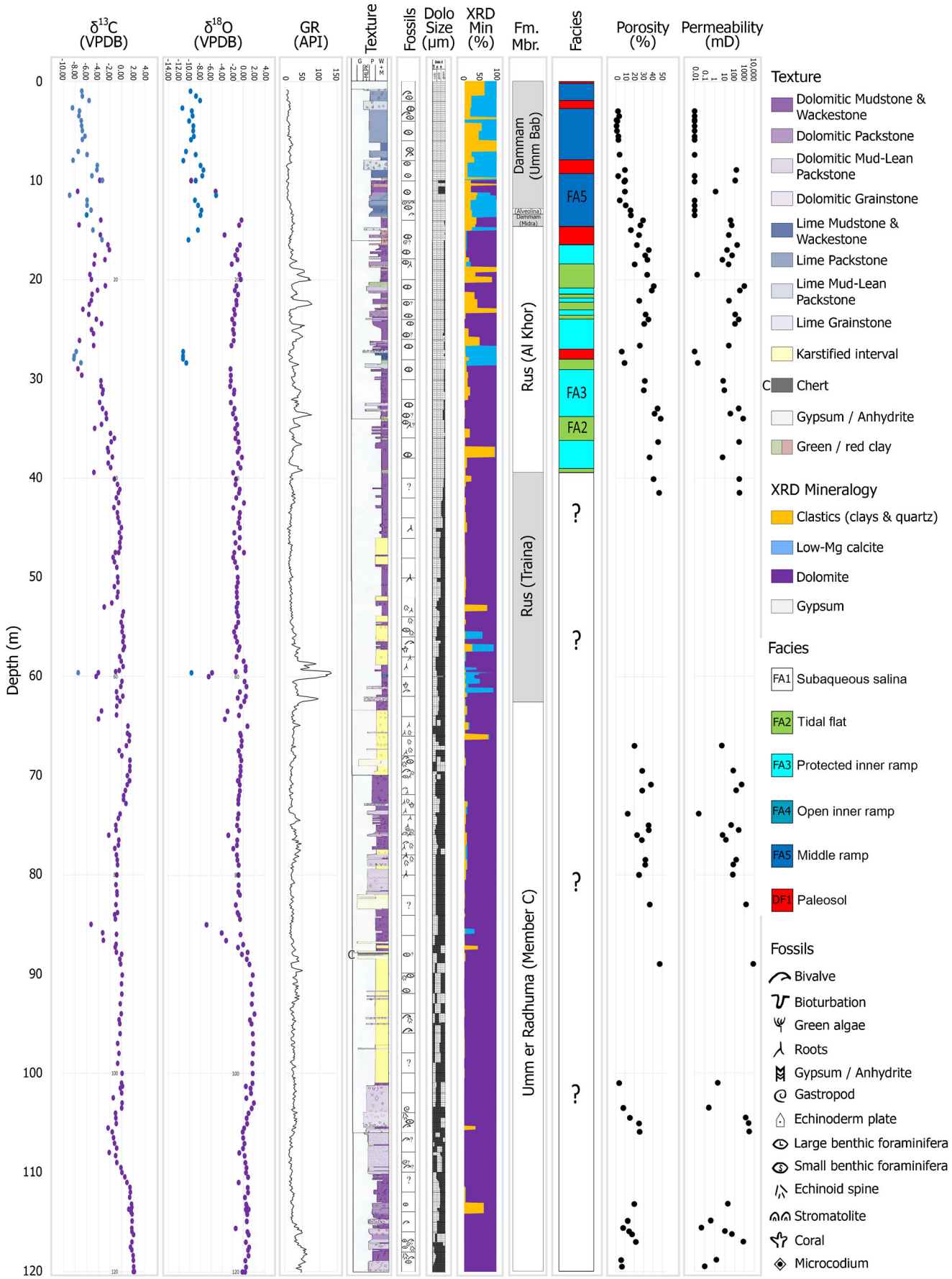
δ13C (VPDB)
δ18O (VPDB)
GR (API)
Texture
Fossils
Dolo Size (µm)
XRD Min (%)
Fm. Mbr.
Facies
Porosity (%)
Permeability (mD)
Depth (m)
Dammam (Umm Bab)
(Alveolina) Dammam (Midra)
Rus (Al Khor)
Rus (Traina)
Umm er Radhuma (Member C)
FA5
FA3
FA2
?
Texture
Dolomitic Mudstone & Wackestone
Dolomitic Packstone
Dolomitic Mud-Lean Packstone
Dolomitic Grainstone
Lime Mudstone & Wackestone
Lime Packstone
Lime Mud-Lean Packstone
Lime Grainstone
Karstified interval
Chert
Gypsum / Anhydrite
Green / red clay
XRD Mineralogy
Clastics (clays & quartz)
Low-Mg calcite
Dolomite
Gypsum
Facies
FA1 Subaqueous salina
FA2 Tidal flat
FA3 Protected inner ramp
FA4 Open inner ramp
FA5 Middle ramp
DF1 Paleosol
Fossils
Bivalve
Bioturbation
Green algae
Roots
Gypsum / Anhydrite
Gastropod
Echinoderm plate
Large benthic foraminifera
Small benthic foraminifera
Echinoid spine
Stromatolite
Coral
Microcodium

◀ **Fig. 6** Borehole 2 core description integrating whole-rock stable isotope composition ($\delta^{18}O$ and $\delta^{13}C$), down-hole gamma-ray (GR), rock texture, fossil assemblage, dolomite crystal size, XRD-based mineralogical composition, formation, and member boundary interpretation, depositional facies interpretation, as well as plug porosity and permeability measurements

Depth interval 60.2–51.0 mbs Rocks of this interval are notably lighter in color than those below. These very-light-brown rocks consist of non-mimetic dolomite. Rocks are interpreted to mostly represent bioturbated packstones and with infrequent lamination. Dasyclad green algae are recognizable allochems, and molds of small benthic foraminifers and molluscs are tentatively identified. The interval is capped by a fractured and brecciated rock with associated crystalline calcite (Fig. 15f).

Depth interval 51.0–26.5 mbs This interval is made of white to light-brown dolomite packstones and wackestones displaying burrow features, wavy-to-straight lamination, and possible ripples. Recovered rocks were significantly disturbed, hampering characterization. Palygorskite is observed to increase from mostly absent at the base of the interval to a common secondary mineral at the top. Dolomitization is mostly non-mimetic, and allochems are only sparsely recognizable. The large benthic foraminifer *Nummulites* was recognized in one thin section (46.2 mbs), but more commonly small benthic foraminifers (miliolid and *Rotalia* sp.) and small bivalve and gastropod molds were identified (Fig. 16a).

Depth interval 26.5–7.7 mbs Off-white and intermittently red-stained bioturbated dolomitic wackestones, mudstones, and minor packstone intervals are interbedded with centimeter-scale palygorskite/illite clay deposits and two notable crystalline limestone beds. Dolomitic and clay-rich rocks are sporadically laminated and include abundant erosive surfaces, sparse mud cracks, and common mud clasts (Fig. 16b). Allochems include small benthic foraminifera (miliolids and rotalid species) and mollusc molds (Fig. 16c). Vugs in dolomitic rocks are commonly lined with clays (16 days). Crystalline limestones include microcodium textures, whereas evidence of original allochems has been diagenetically obliterated (Fig. 16e).

Depth interval 7.7–0 mbs This is composed of cream-colored, brown-stained limestones and dolostones displaying significant recrystallization and karst-related brecciation. Original rock fabric is mostly obliterated, but the presence of Nummulitic packstone is observed and includes lesser numbers of *Alveolina* and *Coskinolina* sp. foraminifera (Fig. 16f), green algae, and molluscs. Palygorskite is a secondary mineral filling karst-related vug.

Bulk stable isotope measurements

Bulk (i.e., whole rock) stable isotopic measurements ($\delta^{13}C$ and $\delta^{18}O$) of carbonate rock samples from boreholes 1 ($n = 163$), 2 ($n = 229$), and 3 ($n = 147$) are plotted separately by depth in Figs. 5, 6, and 7 and cross-plotted as a function of (a) geologic formation and (b) carbonate mineralogy in Fig. 17. As a set, the $\delta^{18}O$ values of rock samples from these strata vary between −12‰ and +2‰, and similarly, the $\delta^{13}C$ values vary between −10‰ and +2‰. The $\delta^{13}C$ and $\delta^{18}O$ values of rocks from the three boreholes generally overly each other (Fig. 17a), whereas the three formations show distinct stable isotopic ranges. Rocks from the Umm er Radhuma (UER) Formation predominantly fall between −2‰ and +2‰ for both $\delta^{13}C$ and $\delta^{18}O$. Rocks of the Rus Formation typically have $\delta^{18}O$ values similar to the underlying UER Formation, whereas $\delta^{13}C$ values range between −10‰ and 0‰. With only a few exceptions, rocks of the Dammam Formation show $\delta^{18}O$ values between −12‰ and −6‰ and invariably have $\delta^{13}C$ values of less than −3‰. When plotted by dominant mineralogy, more distinct trends are apparent (Fig. 17b). Calcitic rocks plot along a trend between −12‰ and −5‰ for $\delta^{18}O$ and −9‰ and −4‰ for $\delta^{13}C$. Dolomitic rocks have higher $\delta^{18}O$ values (−4‰ to +2‰) and more variable $\delta^{13}C$ values (−10‰ to +2‰). $\delta^{18}O$ of silica from silicified carbonate rocks of borehole 1 and borehole 3 were also measured ($n = 4$) (Appendix 2). $\delta^{18}O$ values varied between −2.2‰ and −11.7‰.

Interpretation

Depositional facies and environments

Based on skeletal assemblage, as well as depositional textures, structures, and mineralogy, five depositional facies associations (FA) have been delineated in the three cores recovered for this study. One diagenetic facies association (DA) was also observed. The environments in which the FAs and DA formed are interpreted below.

FA1 Coarsely crystalline, nearly pure, meter-scale beds of gypsum (and minor anhydrite) displaying relict structures of radiating crystal fabric (Fig. 11a-3, c).

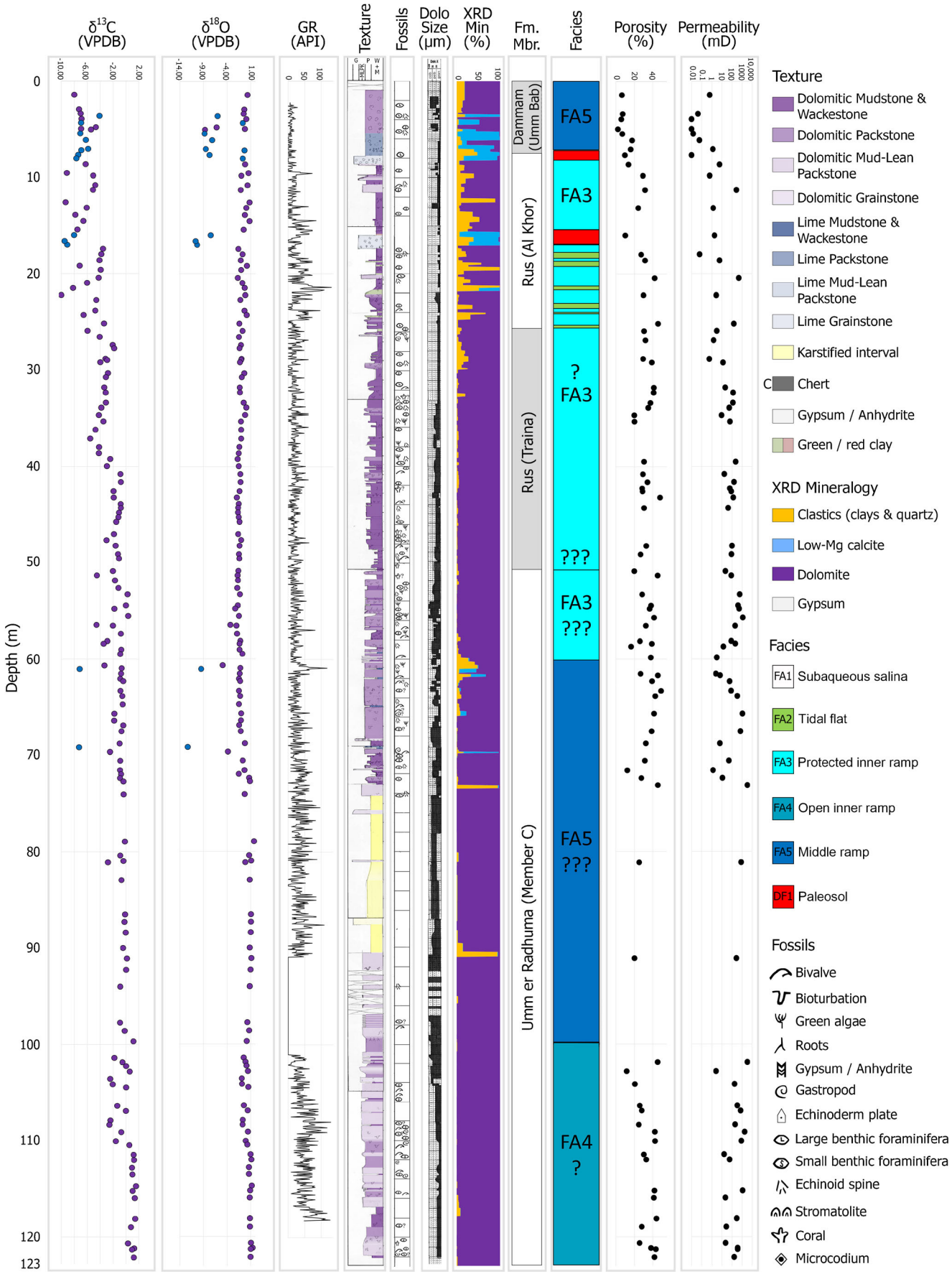
δ13C (VPDB)
δ18O (VPDB)
GR (API)
Texture
Fossils
Dolo Size (µm)
XRD Min (%)
Fm. Mbr.
Facies
Porosity (%)
Permeability (mD)
Depth (m)
Dammam (Umm Bab)
Rus (Al Khor)
Rus (Traina)
Umm er Radhuma (Member C)
FA5
FA3
? FA3
???
FA3 ???
FA5 ???
FA4 ?
Texture
Dolomitic Mudstone & Wackestone
Dolomitic Packstone
Dolomitic Mud-Lean Packstone
Dolomitic Grainstone
Lime Mudstone & Wackestone
Lime Packstone
Lime Mud-Lean Packstone
Lime Grainstone
Karstified interval
Chert
Gypsum / Anhydrite
Green / red clay
XRD Mineralogy
Clastics (clays & quartz)
Low-Mg calcite
Dolomite
Gypsum
Facies
FA1 Subaqueous salina
FA2 Tidal flat
FA3 Protected inner ramp
FA4 Open inner ramp
FA5 Middle ramp
DF1 Paleosol
Fossils
Bivalve
Bioturbation
Green algae
Roots
Gypsum / Anhydrite
Gastropod
Echinoderm plate
Large benthic foraminifera
Small benthic foraminifera
Echinoid spine
Stromatolite
Coral
Microcodium

◀ **Fig. 7** Borehole 3 core description integrating whole-rock stable isotope composition ($\delta^{18}O$ and $\delta^{13}C$), down-hole gamma-ray (GR), rock texture, fossil assemblage, dolomite crystal size, XRD-based mineralogical composition, formation, and member boundary interpretation, depositional facies interpretation, as well as plug porosity and permeability measurements

Interpretation Lack of associated carbonate or siliciclastic "host" sediment indicates these are not sabkha evaporites (e.g., Strohmenger and Jameson 2014). Radiating crystal fabric indicates nucleation from a substrate, likely in shallow water (Warren 2016). Therefore, rocks FA1 are interpreted as subaqueous salina deposits.

FA2 These are mud-rich, fossil-poor, straight, and crinkly laminated, white dolomitic rocks, as well as green clay-rich rocks with red staining (Figs. 10a, 11a-1, 14c, and 16b). Algal mat structures are interpreted in thin sections of these rocks (Fig. 11d), and mud cracks are found in association (Fig. 14d). Rocks of this facies commonly show evidence of early post-depositional reworking and erosion (Fig. 14c and 16b). Rocks of this facies are frequently intercalated with those of FA1 (only in borehole 1) and FA3.

Interpretation Both the presence of interpreted algal mat structures and mud cracks point to formation in intertidal

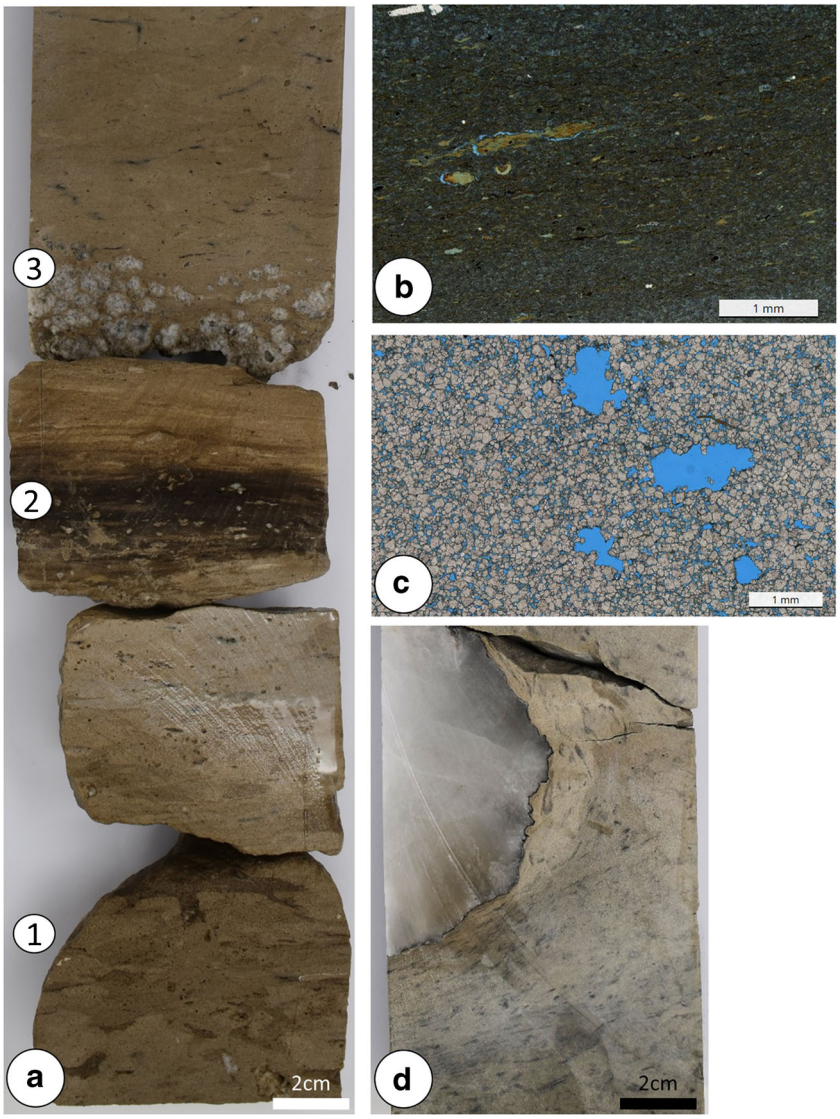

Fig. 8 Images of core from borehole 1. **a** Interval between 124.1 and 123.8. Meter-scale cycles at this depth consist mostly of (1) bioturbated coarsely-crystalline dolostones (interpreted mud-lean packstones) and are typically capped by (2) laminated dolo-wackestones or dolo-mudstones. In some cases, cycle bases show (3) skeletal or intraclast-dominated lags resting directly on underlying cycle caps. **b** Thin section of typical cycle cap (122.94 mbs) with finer dolomite crystals with pore-occluding green/brown palygorskite clays (porosity 42.9% and permeability 109 mD). **c** Thin section of typical cycle base (124.13 mbs) with coarse, clay-free dolomite crystals (porosity 24.4% and permeability 196 mD). **d** Displacive gypsum nodules from 89.6 mbs

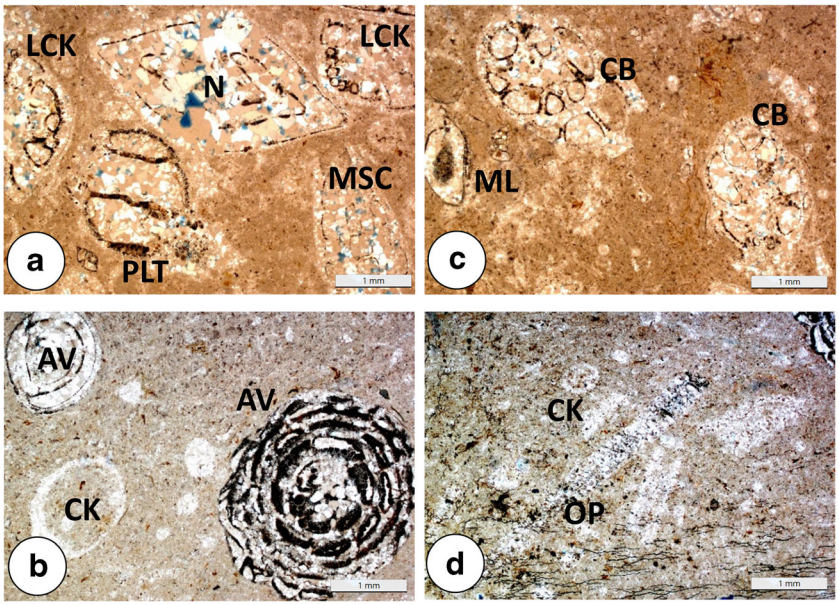

Fig. 9 Plane-polarized (**a**, **c**) and cross-polarized (**b**, **d**) thin-section images of silicified rocks from borehole 1 at 127.6 mbs. Fossils include **a** large benthic foraminifera *Lockhartia* sp. (LCK), *Pseudolituonella* sp. (PLT), *Nummulites* (N), *Miscellanea* sp. (MSC), **b** large benthic foraminifera *Alveolina* sp. (AV), as well as Dasyclad green algae *Cymopolia kurdistanensis* (CK), **c** large benthic foraminifera *Cribrobulimina* sp. (CB) and the small benthic miliolid (ML) foraminifera, and **d** large benthic foraminifera *Opertorbitolites* sp. (OP) as well as Dasyclad green algae *Cymopolia kurdistanensis* (CK)

settings, where laminated sediments are commonly reworked by storms or overprinted by soil-forming processes during exposure (Ebanks and Bubb 1975; Shinn 1983; Pratt and James 1986). Clay-rich intervals observed in this association indicate periodic input of fine, land-derived sediment. Rocks of FA2 are therefore interpreted to represent a low-energy tidal flat environment.

FA3 These are off-white, bioturbated, and uncommonly rippled dolomitic mudstones, wackestones, and packstones rich in small benthic foraminifera (miliolid and rotalid), and including ostracods, as well as small bivalves (Figs. 10b, 11b, 14b, and 16a, c).

Interpretation Low-diversity miliolid-rich assemblages in Paleogene rocks indicate hypersaline or nutrient-rich shallow-water environments within the upper photic zone, where these forms might be associated with algal growth (Geel 2000; Zamagni et al. 2008; Abdel-Fattah et al. 2013; Sarkar 2017). The intercalation of rocks of this facies and those of FA2 would seem to support this association. The light color of these rocks and the ubiquitous presence of diverse burrow features point to well-oxidized pore water conditions. The generally muddy nature of the deposits indicates a lower-energy setting. A shallow, well-lit, but somewhat restricted setting is inferred. In sum, evidence leads to the interpretation of a protected interior ramp or shallow subtidal lagoon setting.

FA4 These are light- to dark-gray bioturbated dolomitic mudlean packstones with subordinate muddier rocks. These deposits are rich in large (centimeter-scale) bivalves and gastropods (Fig. 15a). A variety of small foraminifera (miliolid, textularid, rotalid, and agglutinated) and rare planktonic foraminifers are observed, as well as dasyclad green algae (Fig. 15a–c).

Interpretation The diversity of the assemblage indicates a normal marine deposit within the photic zone. The grain-dominated nature of the rocks points to more energetic settings. FA4 is interpreted as an open shallow subtidal inner ramp setting (e.g., a more energetic equivalent to the "less-restricted lagoon" of Abdel-Fattah et al. 2013).

FA5 These are light- to dark-brown bioturbated dolomitic packstones rich in large benthic foraminifera including species of *Nummulites*, *Lockhartia*, and, less commonly, *Alveolina*. Echinoderms, dasyclad green algae, coral fragments, and both planktonic and small benthic foraminifera are also observed in rocks of this association (Figs. 9, 12c, 15e, and 16f).

Interpretation Both fossil diversity as well as ubiquitous bioturbation indicate normal marine waters and oxygenated pore waters. The consistent presence of mud points to environments commonly below normal wave base. The association of nummulitids and alveolinids has been

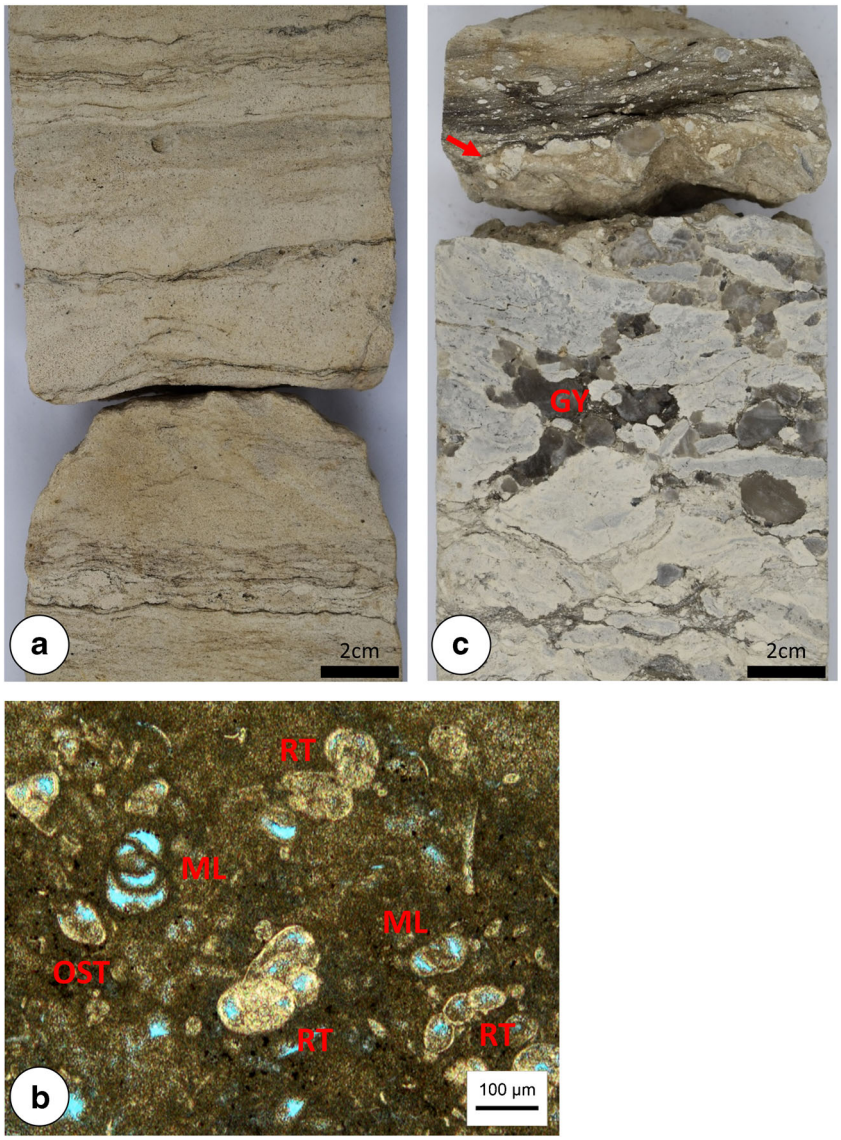

Fig. 10 Images of core from borehole 1. **a** Crinkly laminations observed at 66.7 mbs. **b** Mimetically dolomitized rock from 65.8 mbs showing small miliolid (ML) and *Rotalia* sp. (RT) foraminifera, as well as ostracods (OST). **c** Breccia with a gypsum matrix (GY) at 61.3 mbs overlain by an erosion surface (red arrow) that cuts across grain boundaries

observed previously in Middle Eocene rocks and interpreted to have formed in mid-ramp settings (Van Gorsel 1988), perhaps with lower-energy and reduced light conditions (Sarkar 2017).

DA1 These are gray, highly recrystallized limestones displaying a fabric of aligned calcitic prisms (microcodium) and vugs lined with clay (Figs. 12b and 16e).

Interpretation Microcodium (Esteban and Klappa 1983) is indicative of alteration in well-drained semi-arid soils (Kabanov et al. 2008). Other indications of soil formation include root traces and palygorskite argillans (clay skins) (16d) that are also indicative of well-drained soils (Retallack 2001). Therefore, rocks of DA1 are interpreted to be paleosols.

Lithostratigraphic correlation

Three formations majoritively form the near-surface aquifer rocks of Qatar: the Umm er Radhuma Formation, the Rus Formation, and the Dammam Formation (Cavelier et al. 1970; Abu-Zeid and Boukhary 1984; Abu-Zeid 1991; Boukhary and Alsharhan 1998; Al-Saad 2003; Dill et al. 2003; Al-Saad 2005). In southern Qatar, the base of the Rus Formation is marked by the first presence of bedded gypsum (Al-Saad 2003), corresponding to a depth 61.2 mbs at the borehole 1 location, where a centimeter-thick gypsum bed is observed (Fig. 5). Ten centimeters below the gypsum bed is a brecciated rock overlain by a prominent erosion surface, which cross-cut grain boundaries (Fig. 10c). This disconformity is interpreted to represent the contact between the UER

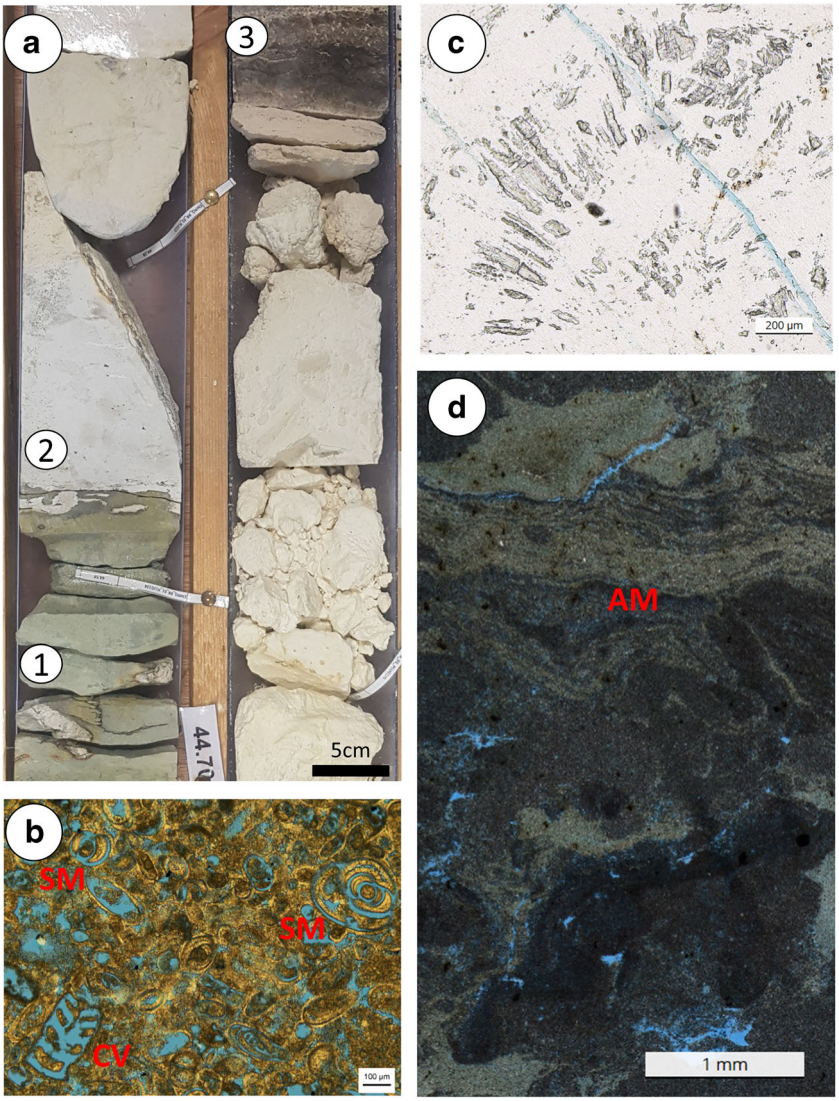

Fig. 11 Images of core from borehole 1. **a** Core photo from 44.7 mbs showing (1) green, palygorskite-rich clay (cycle cap). The top of this clay unit is bored, indicating the presence of a firm/hard-ground, and the boring is infilled with (2) overlying dolomite packstone, representing a cycle base. The packstone passes into (3) a bedded gypsum interval. **b** Thin section image of a dolo-packstone intraclast which has a grainstone texture from 42.73 mbs showing small miliolid (ML) and *Clavulina* sp. (CV) foraminifera. **c** Thin-section image of gypsum bed from 32.53 mbs showing relict radiating crystal habit. **d** Thin-section image of a clay-rich rock from 31.0 mbs. Crinkled laminations are interpreted to represent a disturbed algal mat (AM) structure, which is interbedded with a clay and fine dolomite matrix that bears mud clasts

and the Rus Formations. It is associated with a local gamma-ray peak that can be correlated to a similar peak in borehole 2 at a nearly identical depth (62.4 mbs) where a breccia is also tentatively identified (Fig. 14a) and across which rock textures transition from wackestones to mudstones (Fig. 6). Correlation of the contact between the UER Formation and Rus Formation to borehole 3 is less certain, as the gamma-ray log from this borehole remains mostly low. The correlative boundary was chosen at 51 mbs, where a fractured and brecciated surface is observed (Fig. 15f), across which textures generally fine from mostly packstones to wackestones and mudstones.

The formational boundary between the Rus Formation and the overlying Dammam Formation is marked by a change from dolomitic limestones rich in algae and small benthic foraminifers to shaly and fossiliferous limestones rich in large benthic foraminifera including *Nummulites* and *Alveolina* types (Dill et al. 2003; Al-Saad 2005). This transition is conspicuous in all cores, as fossil remains are well-preserved at this boundary. In borehole 1, the first nummulitic limestones are observed at 14.6 mbs, the underlying rock being recrystallized limestone interpreted as a paleosol (DA1) and as representing a significant exposure event (Fig. 5). Similar transitions are recognized in borehole 2 at 14.6 mbs and borehole 3 at 7.7 mbs (Figs. 6 and 7).

Lithostratigraphic division of the UER in Qatar has only been undertaken in the area of the Dukhan antiform, where Boukhary et al. (2011) divided the formation into three members: (A) shaly marl, (B) marls and limestones, and (C) chert-bearing limestones and, in their most eastward well (their well E), 60 m of dolomitic rocks with evaporites in the upper ~15 m. UER Member C is described as being rich in a diverse

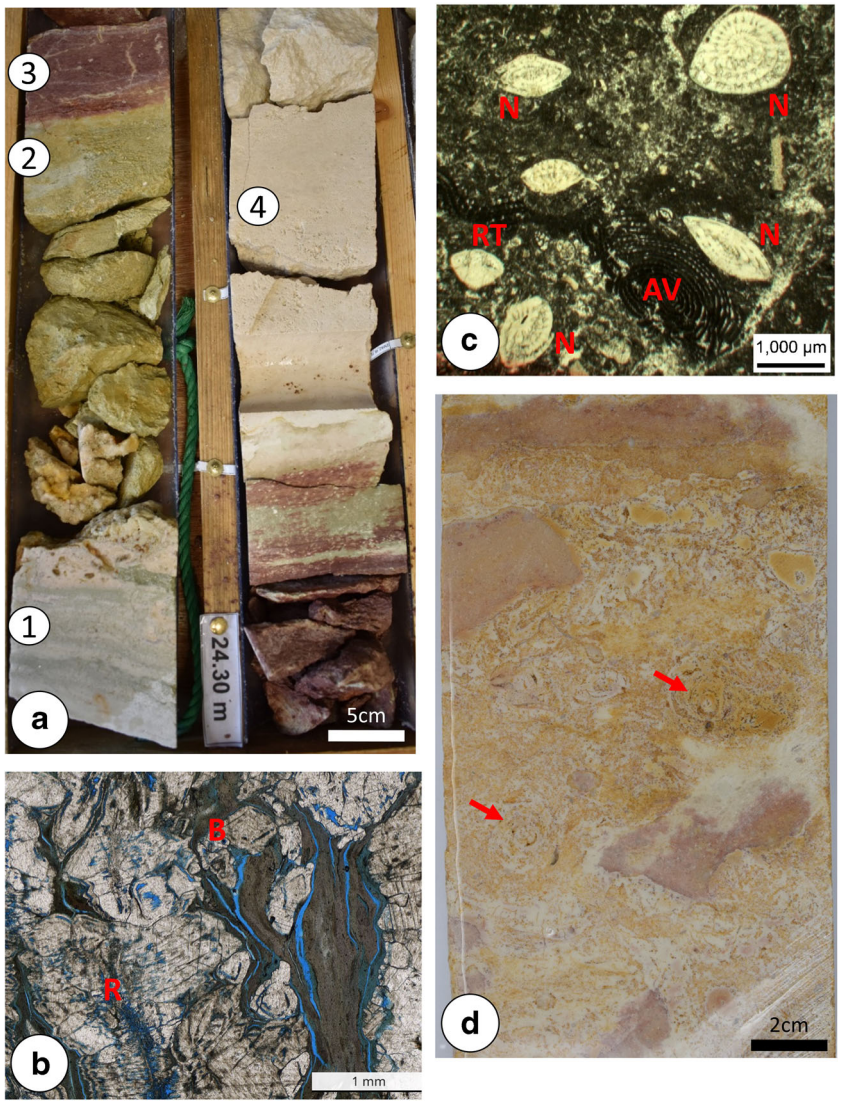

Fig. 12 Images of core from borehole 1. **a-1** Coarse, crystalline calcite overlain by (**a-2**) a green clay-rich interval and (**a-3**) a red clay-rich interval between 24 and 23 mbs. The red clay-rich deposit is overlain by (**a-4**) dolomitic rocks with peloids and small benthic foraminifers. **b** Diagenetic calcite crystals (microcodium textures) at 24.1 with inter-crystalline clay. Both radiating prisms (R) and basal sections (B) of microcodium are apparent. Compare with Esteban and Klappa (1983), their Fig. 69. **c** Packstone with *Alveolina* sp. (AV), *Nummulites* sp. (N), and *Rotalia* sp. (RT) from 14.49 mbs. **d** Centimeter-scale concretions observed at a depth of 9 mbs (red arrows)

assemblage of large benthic foraminifera, particularly various *Lockhartia*, which are also identified amongst the diverse assemblage of large benthic foraminifera observed in a thin, silicified interval of the UER in borehole 1 (Fig. 9). Although rocks of the UER Formation in all three boreholes are almost entirely formed of fossil-obliterative dolomite, these rocks are interpreted to be correlative to those of the UER Member C of Boukhary et al. (2011). This correlation is based on their common stratigraphic position immediately below the Rus, as well as the similar presence of replacive gypsum nodules toward the top of the interval (Figs. 5 and 8d).

The Rus Formation is divided into two members, the Traina and Al Khor (Al-Saad 2003). The Traina Member is designated as being gypsum-bearing, whereas the overlying Al Khor Member is dolomitic limestone. Using this designation, the Traina Member is recognized between 61.2 and 31.2 mbs in borehole 1 (Fig. 5), with the Al Khor Member being represented by the remaining Rus Formation above, including interbedded limestones, dolostones, and clay-rich rocks. Thickly-bedded gypsum in the Rus Formation is only found south, east, and west of a prominent northward-opening "v"-shaped escarpment (Fig. 1) (Eccleston et al. 1981). Cores from boreholes 2 and 3 were recovered north of the escarpment, where gypsum is absent, and so a different designation is required for the Traina equivalent in this region. Both Abu-Zeid (1991) and Boukhary and Alsharhan (1998) recognized three members of the Rus Formation in northern Qatar. Using Abu-Zeid's informal names, they include Member A, a "gypsiferous" facies; Member B, white dolomitic limestones; and Member C, gray chalky limestones interbedded with white dolomitic marls and green claystones. Member A, however, was only found to be "dominantly

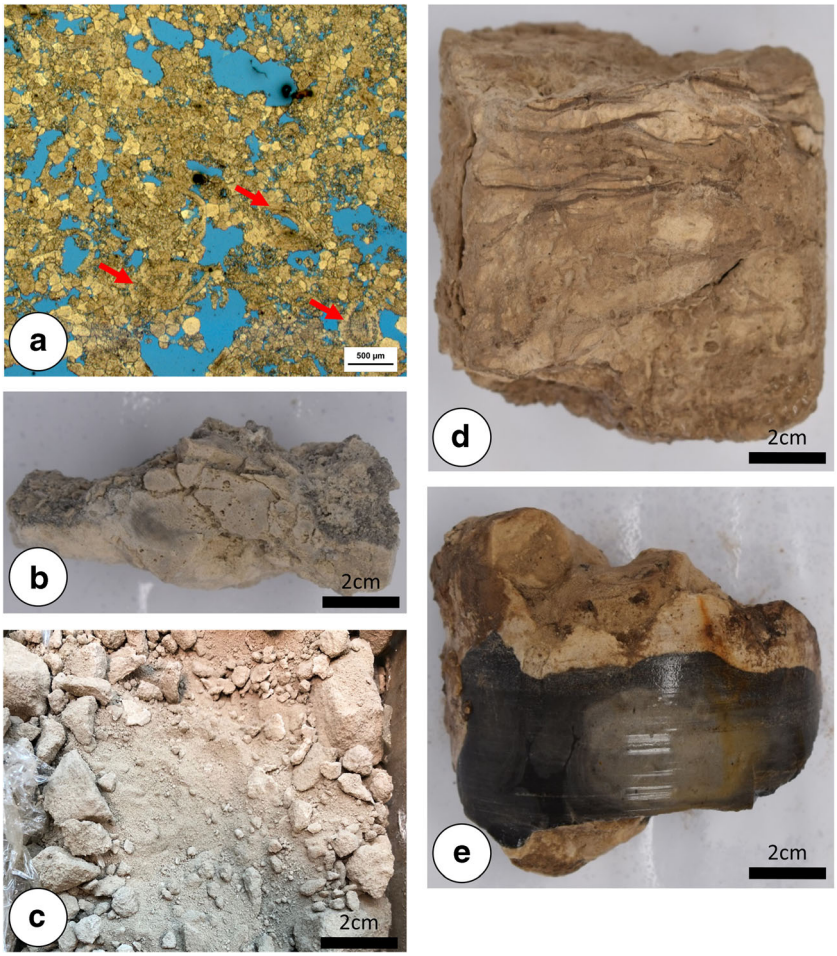

Fig. 13 Images of core from borehole 2. **a** Ghosts of *Nummulites* foraminifera in dolomitized rocks from 117 mbs (red arrows). **b** Interpreted synsedimentary breccia at 105.4 mbs. **c** Sediments in core at a depth of 99.0 mbs. **d** Intact rock within interval dominated by dolomitic sediment displaying horizontal lamination. **e** Chert-replaced interval in dolomitic sediment at 88.3 mbs

gypsiferous" in northwestern Qatar, west of the escarpment, and so is equivalent to the Traina Member described above. Bulk-rock XRD analyses from of rocks from boreholes 2 and 3 (Appendix 1) indicate no gypsum is found in either core in any of the penetrated formations. Therefore, in cores 2 and 3, and north of the escarpment in general, Abu-Zeid's (1991) Member B (white dolomitic rocks) is likely time-equivalent to the Traina Member south of the escarpment, whereas rocks of Member C (limestones interbedded with dolomites and claystones) are equivalent to the Al Khor Member. This designation is useful in that, north of the escarpment, the transition from the Traina Member to the Al Khor Member can clearly be picked based on gamma-ray log, with the Al Khor Member showing generally higher readings and greater variability (Figs. 6 and 7), reflecting the presence of illitic clays. The transition from the Traina to the Al Khor Member in boreholes 2 and 3 is picked at the first bedded clay deposit (39.5 and 26.0 mbs, respectively).

The Dammam Formation, with its extensive exposure across Qatar, has been divided into several members (Cavelier et al. 1970; Cavalier 1975; Al-Saad 2005) (Fig. 18a). The lowest member, the meter-thick, fossiliferous, Rujm Aid Member, is only observed in borehole 1 (13.6–14.6 mbs) and is disconformably (based on the karstified surface observed at the contact (Fig. 18b)) overlain by the Midra Shale. The Midra Shale is composed of two distinctive beds (Al-Saad 2005) of brown-flecked white carbonate rock (Fig. 18c) or claystone with wavy lamination (Fig. 18d) separated by a thin white bed of more pure carbonate (located at a depth of 12.5 in Fig. 18a). The mineralogy of the Midra Shale Member is mixed, and at the Borehole 1, location includes a dolomitic lower bed and calcitic upper bed, both of which bear significant percentages of palygorskite clays (Fig. 5). The Midra Shale is only observed in boreholes 1 (10.8–13.65 mbs) and 2 (13.7–14.6 mbs) and in both locations is capped by the Alveolina Member (Fig. 18d), which is thin (~ 0.5 m) but bears conspicuous *Alveolina* benthic foraminifera. Similar to the Rujm Aid/Midra contact, the contact between the Midra Shale Member and the Alveolina Limestone Member is erosive and appears

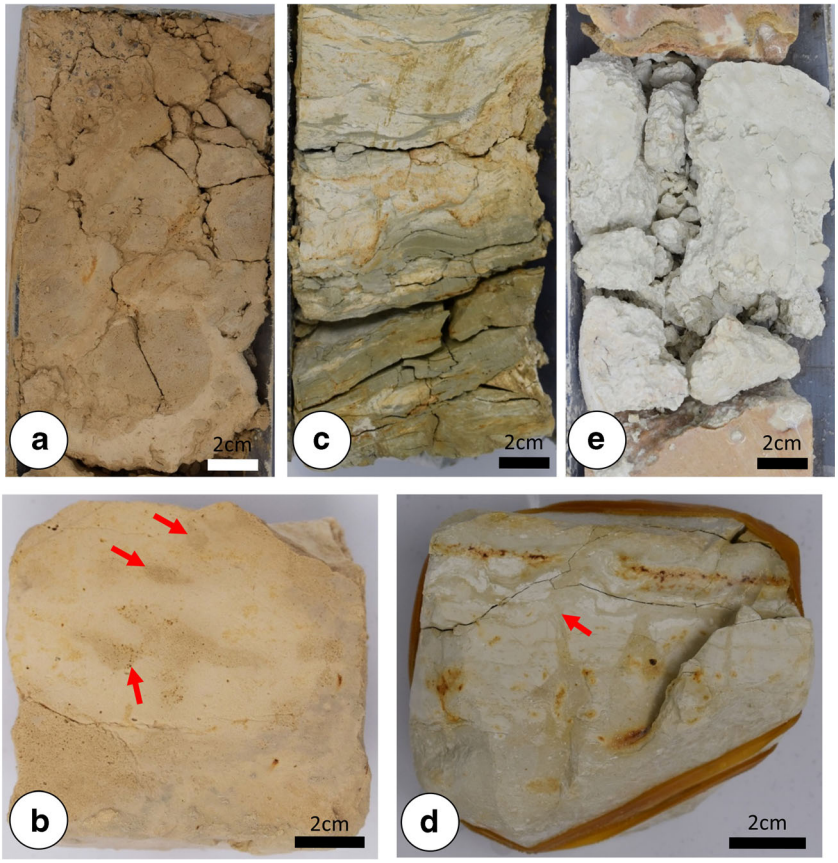

Fig. 14 Images of core from borehole 2. **a** Interpreted synsedimentary breccia at 62.4 mbs. **b** Dolomitic mudstone at 49.0 mbs with more coarsely dolomitized burrow structures (arrows). **c** Reworked laminated deposits rich in dolomite (white) and illitic clay (green) at 34 mbs. **d** Interpreted mud cracks (arrow) in dolomitic mudstones at 18 mbs. **e** Recrystallized limestones at 10 mbs with large vugs filled by white palygorskite clay

disconformable (Fig. 18d). Finally, the Umm Bab is the capping Dammam Formation Member in all three boreholes. In boreholes 1 and 2, it is observed above the Alveolina Member at depths of 10.6 and 13.5 mbs, respectively, and in borehole 3 resting disconformably on the Rus Formation at 7.7 mbs. The Umm Bab Member in all locations bears a significant percentage of clay (commonly greater than 20%) and is otherwise limestone in boreholes 1 and 2 but partially dolomitized in borehole 3 (Figs. 5, 6, and 7). The chert-bearing Abaruq Member is not recognized in any of the boreholes, being confined to outcrops in western Qatar (Al-Saad 2005).

Stable isotopes

The range of $\delta^{18}O$ and $\delta^{13}C$ values for bulk carbonate samples in this study is comparable to those reported for the "Upper Dammam" Formation by Holail et al. (2005) for samples from drill wells in SE Qatar (Fig. 17a). In the Holail et al. (2005) study, $\delta^{18}O$ values for dolomitic samples ranged between 0‰ and +3‰, whereas $\delta^{13}C$ values were more variable and formed distinct groups including "type 1 dolomite" between −6‰ and −10‰ and "type 2 dolomite" between 0‰ and −4‰. Similar to calcitic rocks from this study, calcite cements reported by Holail et al. (2005) had more negative and variable $\delta^{18}O$ values (−10‰ to −5‰) but $\delta^{13}C$ values similar to the accompanying dolomites (−2‰ to −8‰).

With respect to stable isotopic composition, type 2 dolomite of Holail et al. (2005) is similar to both the dolomite of the UER Formation in general and in boreholes 2 and 3 that of the lower portion of the Rus Formation in this study (Figs. 6, 7, and 17a). Holail et al. (2005) interpreted such dolomite with relatively high $\delta^{18}O$ and $\delta^{13}C$ values to be reflective of dolomitization involving "normal" oxygenated marine water. The $\delta^{18}O$-$\delta^{13}C$ field for UER and lower Rus Formation dolomites from this study approach those reported by Saller (1984) for Eocene-age rocks interpreted to have been dolomitized in "normal marine" waters of the Enewetak Atoll during the Miocene (Fig. 17), supporting the Holail et al. (2005) interpretation.

Holail et al. (2005) interpreted dolomite with relatively high $\delta^{18}O$ but lower $\delta^{13}C$ values (their type 1 dolomite) to be reflective of dolomitization involving marine water undergoing sulfate reduction, with more negative carbon being supplied to dolomitizing waters by degrading organic matter in the sediment. Dolomites

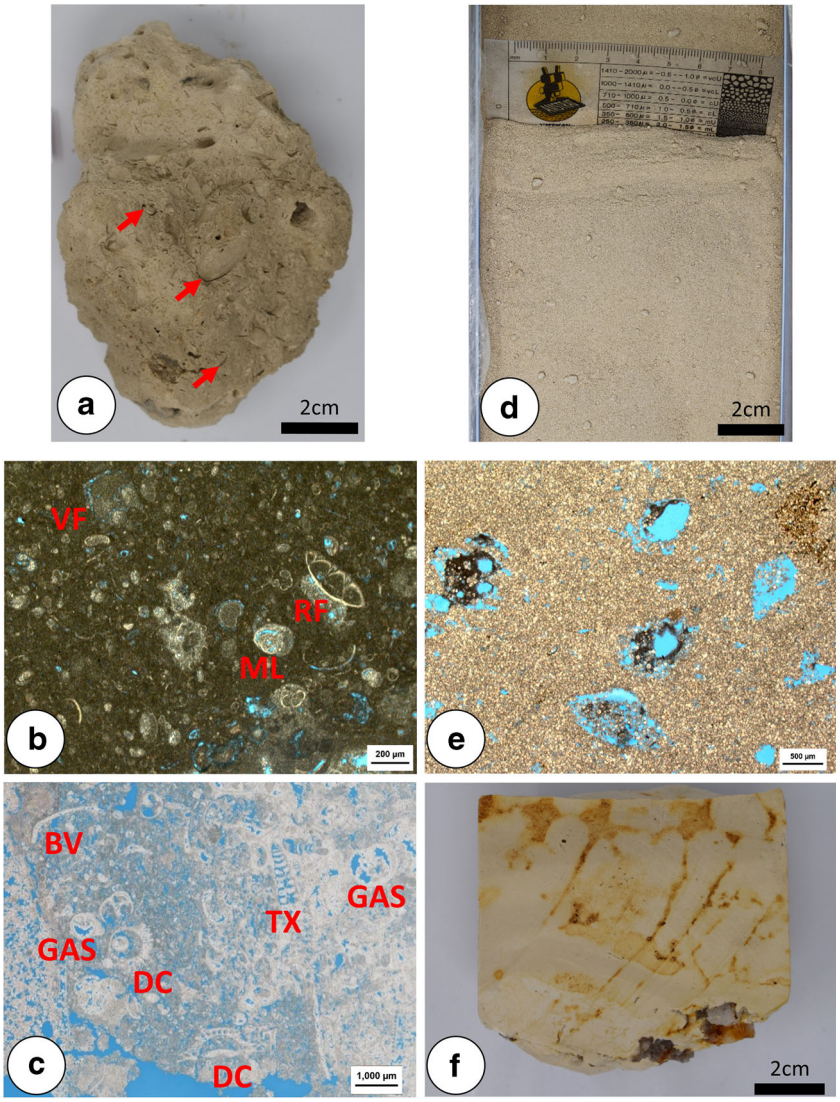

Fig. 15 Images of core from borehole 3. **a** Bivalve molds (red arrows) in rock from 110.25 mbs. **b** Thin-section image of a packstone from 114.73 mbs showing the benthic foraminifer *Rotalia* sp. (RF), the agglutinated foraminifer *Valvulinerid* sp. (VF), as well as small miliolids (ML). **c** Thin-section image of a packstone from 108.05 mbs showing bivalves (BV), gastropods (GAS), dasyclad green algae (*Clypeina* sp.) (DC), and a textularia foraminifer (TX). **d** Fine sand composed of dolomite crystals at 79.0 mbs. **e** Thin section of fossil molds in dolomitized rocks from 69.4 mbs interpreted to form from dissolution of large benthic foraminifera tests. **f** Fractured and brecciated rock at 51.0 mbs

with similar isotopic ranges from this study are found mostly in the Rus Formation but also in the Dammam Formation (Fig. 17a). Whereas the Holail et al. (2005) interpretation cannot by completely discounted based on this study, in samples from all boreholes, the $\delta^{13}C$ values of dolomite in the Rus Formation decrease upward to minimums below interpreted long-term meteoric exposure surfaces (facies DA1). It is therefore interpreted that the more negative carbon in these dolomites are reflective of the incorporation of CO_2 associated with the degradation of organic matter in soils. The $\delta^{18}O$ values in these dolomites are similar to those interpreted to have formed in normal marine waters (UER dolomites). Therefore, seawater incorporating soil-derived organic carbon may have been the dolomitizing solution. That stated, more recent resetting of the oxygen isotopic composition cannot be discounted.

Finally, Holail et al. (2005) interpreted the calcitic cements from their study to have formed from meteoric waters during exposure by lowering sea level. The common association of calcitic rocks in this study with interpreted exposure surfaces supports this interpretation (Figs. 5, 6, and 7). As with the dolomitic rocks in the upper Rus Formation, the more negative carbon in the calcitic rocks is likely supplied through the degradation of soil-derived organic matter. A negative shift in the $\delta^{13}C$ of carbonate rocks is a common effect of meteoric exposure (James and Choquette 1990). The low $\delta^{18}O$ values for the calcitic rocks are not reflective of those of recent meteoric waters, which generally fall between −2‰ and +2‰, close to seawater values (IAEA 1992). Based on regional speleothem studies however, calcitic meteoric cements with $\delta^{18}O$ values between −12‰ and −4‰ are common during interglacial periods, when the intertropical convergence zone shifts northward,

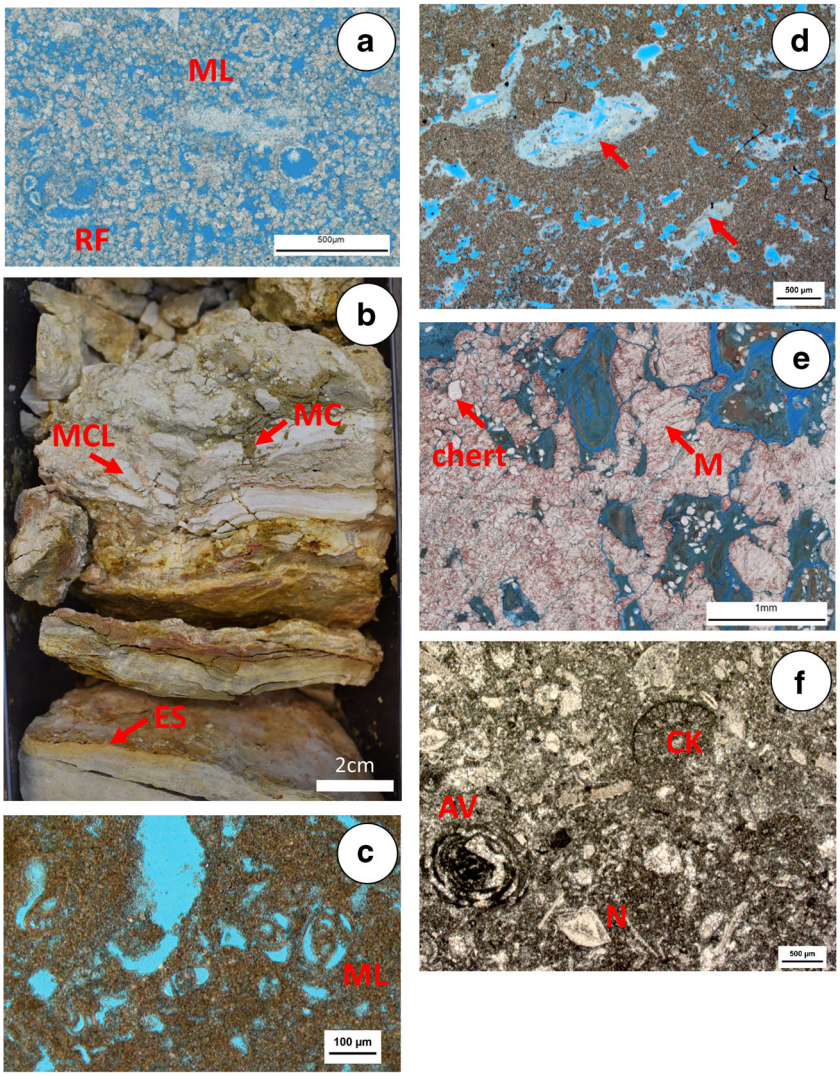

Fig. 16 Images of core from borehole 3. **a** Thin section showing small benthic foraminifera fossils in dolomitized rocks from 33.6 mbs including rotalid (RF) and miliolid types (ML). **b** Image of core from 19.5 mbs showing interpreted erosional surfaces (ES), mud cracks (MC), and mud clasts (MCL). **c** Thin-section image of interpreted packstone at 18.6 mbs rich in miliolid foraminifers (MF). **d** Thin-section image of dolomitic rocks containing clay coatings (argillans; red arrows) from 11.3 mbs. **e** Thin-section image of a recrystallized limestone from 17.0 mbs showing radiating microcodium textures (M). White crystals are of chert. **f** Thin-section image of rock from 5.47 mbs showing large benthic foraminifers including *Nummulites* sp. (N), *Alveolina* sp. (AV), and *Coskinolina* sp. (CK)

bringing more depleted monsoonal waters to the region (Fleitmann et al. 2004). A northward shift of the inter-tropical convergence zone has been inferred during the Middle Eocene based on studies of eolian sediment in cores recovered from the northern Pacific Ocean (Pettke et al. 2002).

The positive correlation observed between $\delta^{13}C$ and $\delta^{18}O$ for calcites in this study seems to be reflective of the degree of alteration. Calcitic rocks with the most negative $\delta^{13}C$ and $\delta^{18}O$ values are commonly those that display coarse recrystallization (e.g., sample in Fig. 12b had measured $\delta^{13}C$ and $\delta^{18}O$ values of −8.6 and −10.4, respectively). The neomorphosed rocks that retained their depositional textures are commonly less negative (e.g., sample in Fig. 12c had measured $\delta^{13}C$ and $\delta^{18}O$ of − 6.1 and −8.6). Therefore, the positive isotope trend could reflect the degree of rock-water interaction, with coarsely-crystalline rocks having greater interaction with meteoric waters, and neomorphosed rocks having less, retaining a greater portion of their isotopic composition from that prior to exposure. Alternatively, the trend could reflect the mixing of marine and meteoric waters below exposure surfaces (James and Choquette 1990) with more marine waters having higher $\delta^{18}O$ values and less soil-derived carbon. Although a complete paragenetic sequence was not undertaken for this study, it is clear from petrographic relationships that the recrystallization of these rocks is multi-generational, with examples of recrystallized limestones having been dolomitized (Fig. 19a) and dolomitized rocks undergoing calcitization (Fig. 19b).

Four samples of silicified carbonate rocks were chosen for $\delta^{18}O$ analyses (Appendix 2), including the decimeter-thick silicified interval in the UER of borehole 1 (Fig. 9). A similar chert bed was found in the UER of boreholes 2 and 3 (Fig. 13e). Samples of chert from the Dammam Formation of borehole 3 were also

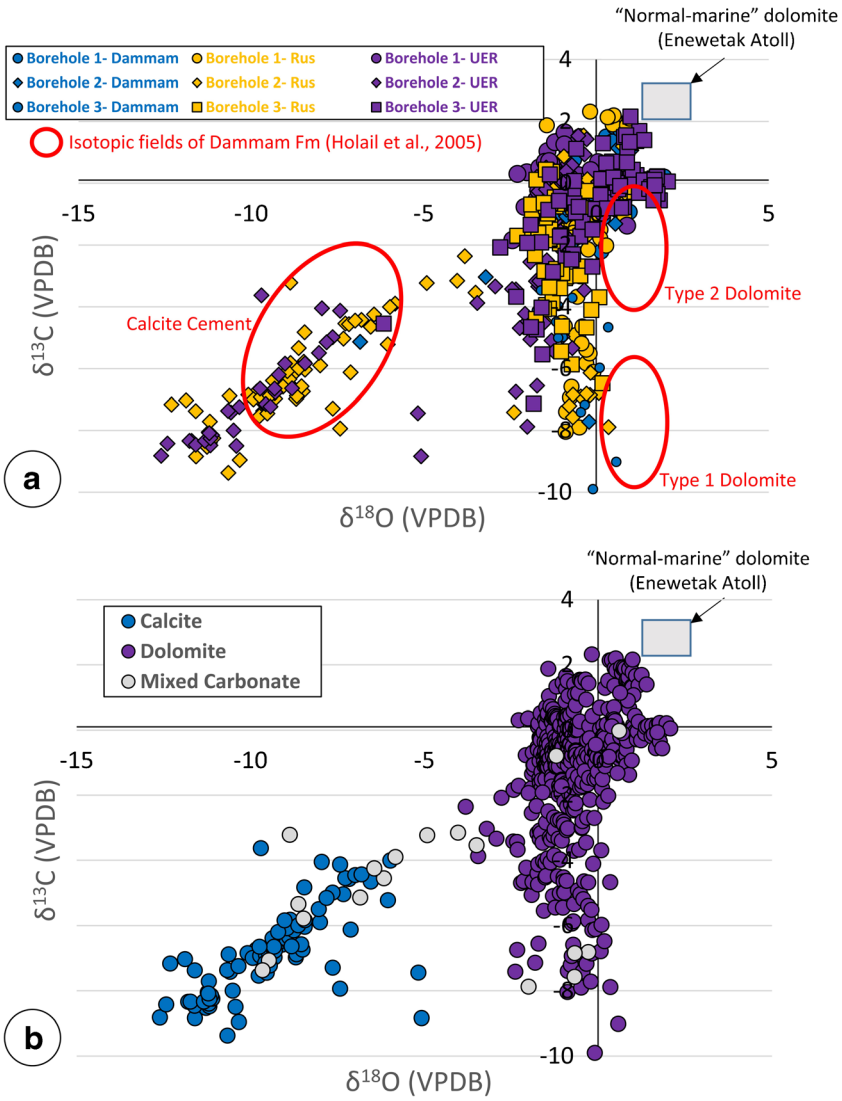

Fig. 17 Cross-plot of whole-rock $\delta^{18}O$ and $\delta^{13}C$ measurements on carbonate rocks from this study as a function of **a** core number and formation and **b** "dominant" carbonate mineralogy, as defined by having greater than 95% either calcite or dolomite based on XRD or by observation using nearest thin section. Samples with greater than 5% of both dolomite and calcite are also plotted as "mixed carbonate." Fields for Eocene rock interpreted to have been dolomitized in "normal marine" water during the Miocene by Saller (1984) are shown in gray box. Isotopic fields of Holail et al. (2005) for the Qatar Dammam Formation are shown with red ovals

analyzed. $\delta^{18}O$ of all chert samples varied between −2.2‰ and −11.7‰, similar in spread to that of limestones described above (−5‰ to −12‰), implying that the chert also formed in meteoric waters. This is supported by the commonly observed association between paleosol formation and chert presence in many Rus Formation and Dammam Formation rocks (Fig. 16e). It is also supported by isotopic studies of chert by Knauth and Epstein (1976), which indicate that, assuming near-surface temperatures of precipitation (20–40 °C), waters forming the chert would be between 0‰ and −12‰ SMOW, pointing to a meteoric origin (e.g., Gao and Land 1991).

Sequence stratigraphic correlation

With respect to sequence stratigraphy (Van Wagoner et al. 1988), the UER, Rus, and Dammam Formations all fall within Arabian Plate Megasequence 10 (AP10) of Sharland et al. (2001), which is bounded by a basal hiatal surface capping the underlying Cretaceous deposits and a capping hiatal surface above by the Dammam Formation. Sharland et al. (2001) identified two major flooding surfaces within AP10, one at the base of the UER Formation (Pg10 MFS), which was not penetrated by any of the boreholes in this study, and one in the Midra Shale Member of the Dammam Formation (Pg20 MFS) (Figs. 4 and 20). Whereas Sharland et al. (2001) did not assign sequence stratigraphic orders to these surfaces, using their interpretation AP10 includes two major sequences, which are herein designated as sequences PG10 and PG20. The sequence boundary below the Midra Shale Member that divides PG10 and PG20 was not assigned by Sharland et al. (2001). Two candidates for this bounding unconformity are found within the cored

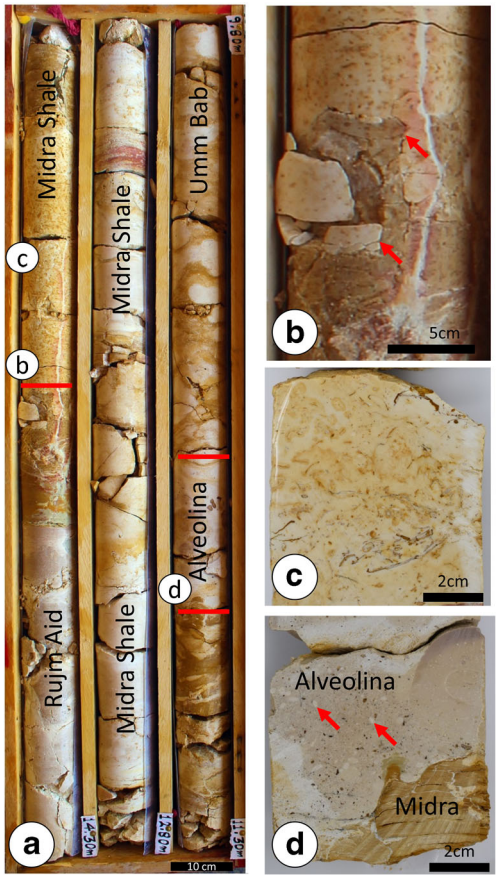

Fig. 18 **a** Image of whole core (borehole 1, 9.8–14.3 mbs) showing members of the Dammam Formation. Red lines denote contacts between members. Locations of images b–d are shown on whole core image. **b** Whole-core image of contact between Rujm Aid Member and the Midra Shale Member. Arrows point to erosive and karstified contact. **c** Split-core image from at 13.4 mbs showing distinctive brown-flecked carbonate of the Midra Shale Member. **d** Image of contact in split-core between the Midra Shale and the Alveolina Members. Arrows point to *Alveolina* sp. benthic foraminifera. Contact is erosive and karstified

interval, both associated with the Rus Formation (Al Khor Member). The first is represented by highly recrystallized rocks bearing microcodium textures (Fig. 12a, b) at a depth of 24 mbs in borehole 1 (Fig. 5) and the second being similarly altered rocks capping the Rus Formation at 14.8 mbs in borehole 1. Both surfaces can be correlated to boreholes 2 and 3, being assigned above similarly altered rocks (Fig. 20). Because the exposure-related alteration of the lower candidate appears more penetrative in all wells based both on core observations and the depth of the associated $\delta^{13}C$ deflection, it is interpreted that this represents the more significant hiatus and by inference the most basinward shift in relative sea level. A designation of this surface as Pg20 SB is therefore assigned (Fig. 20). If this is correct, the interval of the UER Formation penetrated by the three boreholes in this study represents the transgressive/early highstand deposits of the PG10 Sequence. The Rus Formation represents both the late highstand of the PG10, as well as the lowstand (represented as exposure) and early transgressive of the PG20 Sequence. Whereas the Dammam Formation represents the late transgressive and highstand of the PG20 Sequence. This is broadly reflected in the facies tracts, with the UER and Dammam Formations being formed of mostly open ramp deposits (times of high accommodation) and the Rus Formations being rich in protected-lagoonal and tidal flat-deposits (times of low accommodation) (Figs. 5, 6, and 7).

Due to obliterative dolomitization, as well as recrystallization and karstification during meteoric diagenesis, a highly detailed sequence stratigraphic interpretation of these strata is not possible. Candidates for higher-order sequence boundaries (inferred exposure surfaces representing unconformities that can be correlated across the cored intervals) can be offered using the lithostratigraphic observations in concert with bulk stable isotopic trends. Surfaces that top the UER and Rus Formations both show evidence of disconformity (e.g., brecciation, fracture, erosion, recrystallization, and cementation related to meteoric exposure; Figs. 10c, 13b, 14a, and 15f) in all cores. Therefore, these surfaces are interpreted to represent higher-order sequence boundaries relative to Pg20 SB (Fig. 20). In general, the UER Formation is highly altered by obliterative dolomitization, and so assignment of sequence boundaries within the formation carries more uncertainty. One conspicuous feature observed in the UER Formation in all boreholes is a decimeter-thick interval of chert (Figs. 9 and 13e). This bed was recognized by Eccleston et al. (1981) as being continuous and mappable across eastern and southern Qatar. In the Rus Formation, replacive chert crystals are very commonly found in association with diagenetic calcites interpreted to have formed during meteoric exposure (Fig. 16e). Additionally, isotopic analyses of the chert bed indicate that it formed in meteoric waters. We therefore speculate the continuous chert horizon was precipitated in association with a paleo-water table, which was established prior to the coarse dolomitization of UER rocks based on the retention of skeletal ghosts (Fig. 9). If it is assumed that the chert bed represents an originally relatively-flat water table that mimicked a related exposure surface above, it is useful as a stratigraphic indicator and guide for purposes of correlation. The depth of the chert layer is shown in Fig. 20 for all boreholes. An associated exposure surface above the chert bed is picked based mostly on $\delta^{13}C$ deflection (informally designated Intra UER SB (2)). Finally,

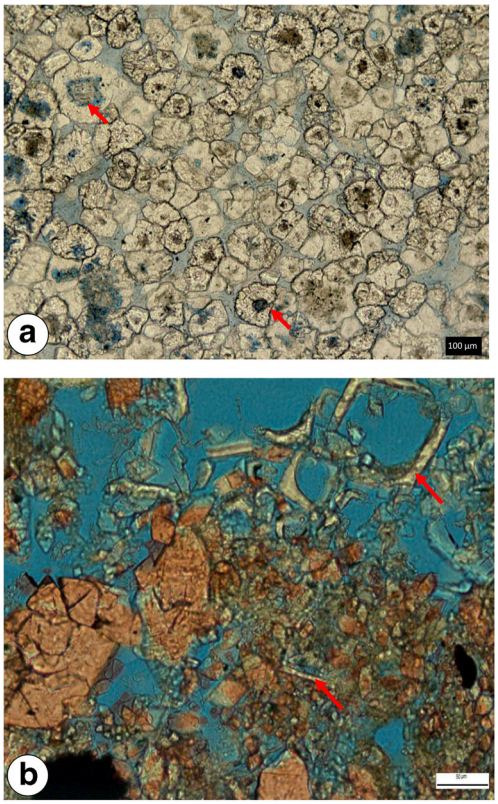

Fig. 19 **a** Ghosts of microcodium structures (red arrows) in a dolomitized rock from the Umm Bab Member of the Dammam Formation taken from a cave near borehole 1 location. **b** Example of calcitization of dolomitized rocks. Calcite is stained with alizaran red. Rims of dolomite rhombs (red arrow) are still present (unstained). Arrow at the base of image shows dolomite rim being replaced by calcite. Many of the stained calcite crystals also retain rhombic shapes of the dolomite precursor mineral

Intra UER SB (1) was inferred based on the occurrence of a blackened and brecciated interval in borehole 2 at 99.7 mbs, which is interpreted to indicate exposure, and across which a facies change is perhaps observed (Fig. 7). This surface is tentatively correlated to borehole 3 based on $\delta^{13}C$ deflection. An equivalent surface is not observed in borehole 1 and so interpreted to fall below the penetrated interval.

Controls on aquifer flow and storage properties

Figure 21 shows porosity and permeability plots for plugs taken from cores of boreholes 1, 2, and 3. The poro-perm clouds for rocks from each borehole generally overly (Fig. 21a), with porosities ranging from less than 5% to greater than 45%, and permeabilities from 0.01 mD to greater than 1000 mD. Plotted by formation (Fig. 21b) demonstrates that the Dammam Formation typically has relatively low porosities (less than 20%) and very low permeabilities (less than 1 mD). The UER and Rus Formations are much more variable but generally show porosities of greater than 10% and permeabilities greater than 1 mD. An examination of poro-perm distribution as a function of dominant mineralogy is more revealing (Fig. 21c). Calcitic rocks (which are common in the Dammam Formation) typically show low porosity (< 20%) and permeability (< 1 mD). Petrographically, this is explained by two observations. First, in rocks that have undergone significant recrystallization by meteoric diagenesis (microcodium-bearing rocks), the fabric is that of coarse interlocking crystals, with vugs being filled by clay (Figs. 12b and 16e). These diagenetic crystals show no petrographic evidence of micropores such as blue haze, and so, most samples fall below the global microporosity trend of Fullmer et al. (2014) and Kaczmarek et al. (2015). In some cases, associated vugs are not filled with clay, and these samples show elevated permeabilities (> 100 mD) but low porosities (< 10%). Second, where depositional fabric is retained, calcitic rocks are invariably mud-bearing (typically packstones) (Figs. 5, 6, and 7), and the depositional matrix precludes significant macroporosity development.

Dolomitic rocks have generally higher but more variable porosities and permeabilities than the limestones. In cases where these rocks are relatively clay-free, they display a between-crystal pore system (e.g., Fig. 8c) with poro-perm ranges that generally fall above the global microporosity trend (Fig. 21c). When clay content of dolomite reaches greater than ~3% (based on XRD), the clay effectively occludes the pore throats (e.g., Fig. 8b) and the poro-perm generally falls on or below the microporosity line. Dolomite crystal size does not play an obvious role in determining aquifer quality in these rocks. For instance, in the UER formation of borehole 1, observed dolomite crystal size generally correlates poorly with measured porosity and permeability trends (Fig. 5); however, permeability can be observed to lower in intervals where clay content increases.

Discussion

If the sequence stratigraphic correlation is correct, it indicates a significant thickening of the UER strata toward the south of Qatar. Such an interpretation is supported by regional paleo-environmental maps (Fig. 22) (Tai et al. 2016) that point to the existence of a Late Paleocene basin immediately south of Qatar, which was only connected to the Zagros foreland basin in the north

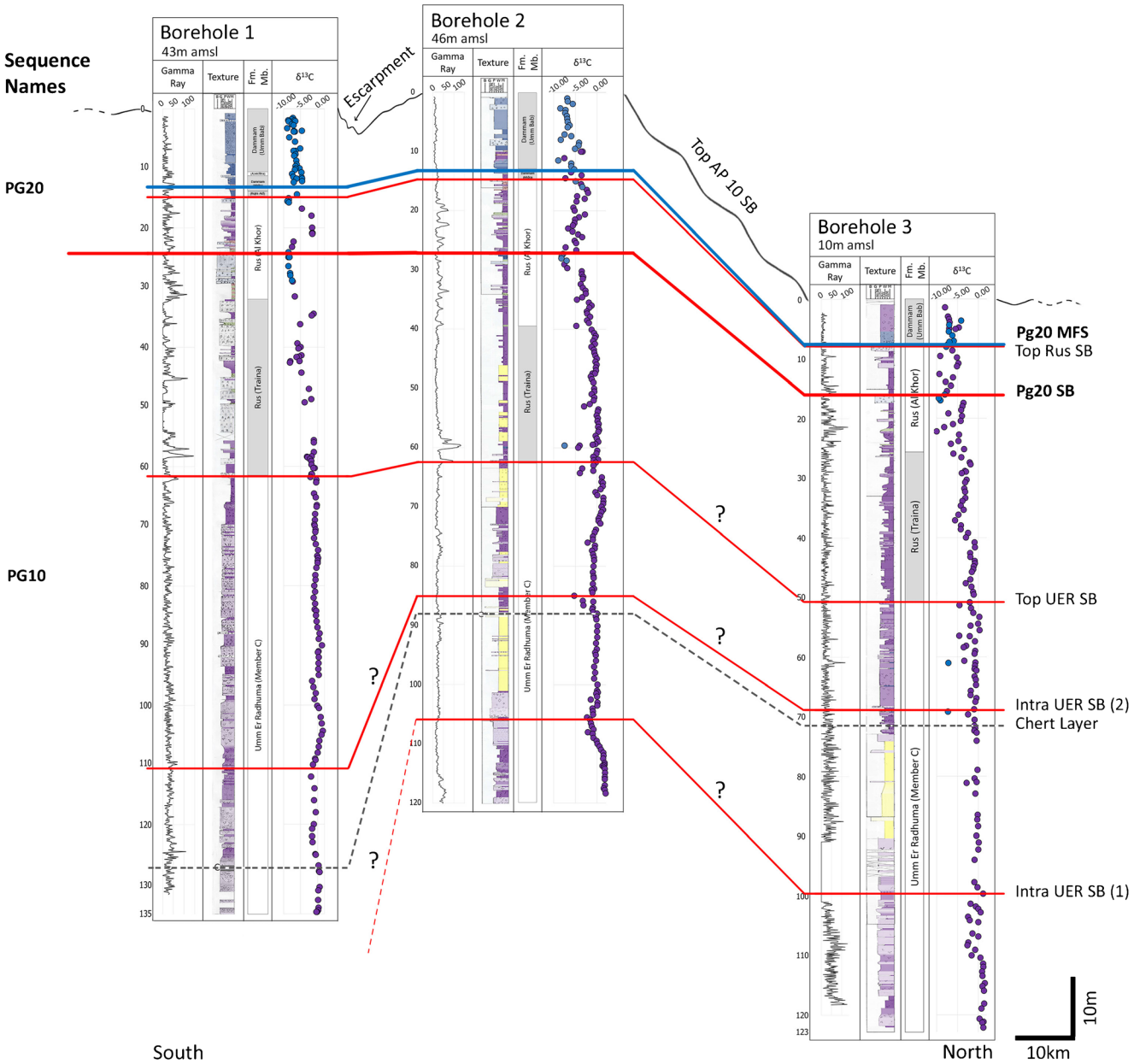

Fig. 20 Sequence stratigraphic correlation using cores from boreholes 1, 2, and 3 (see text). Core descriptions are hung relative to top-borehole elevation. PG10 and PG20 are sequences designated within the AP10 megasequence of Sharland et al. (2001). amsl: above mean sea level

by a narrow seaway. Further support for increased accommodation south of Qatar during the Early Eocene comes from the observation that the Rus Formation also thickens significantly in that direction (Eccleston et al. 1981). The observation that the Traina Member of the Rus Formation is gypsum-bearing in southern Qatar, but not to the north, argues both for the existence of separate basins, and for the southern basin being more restricted.

Rivers and Larson (2018) concluded that a northward-opening "V"-shaped structure in southwest Qatar, defined by the presence of the Miocene Dam Formation and the Pliocene Hofuf Formation (Figs. 2 and 3), was the product of activation and reactivation of high-angle normal faults during the Neogene. A similar northward-opening "V"-shaped escarpment in central Qatar (Fig. 1b) is inferred to be genetically related to the structures in the southwest and likely reflects the presence of similar high-angle normal faults. The location of this central escarpment conforms well to the contact in the Rus Formation (Traina Member) between gypsum-bearing rocks to the south and gypsum-free equivalents to the north observed by Eccleston et al. (1981), implying that such

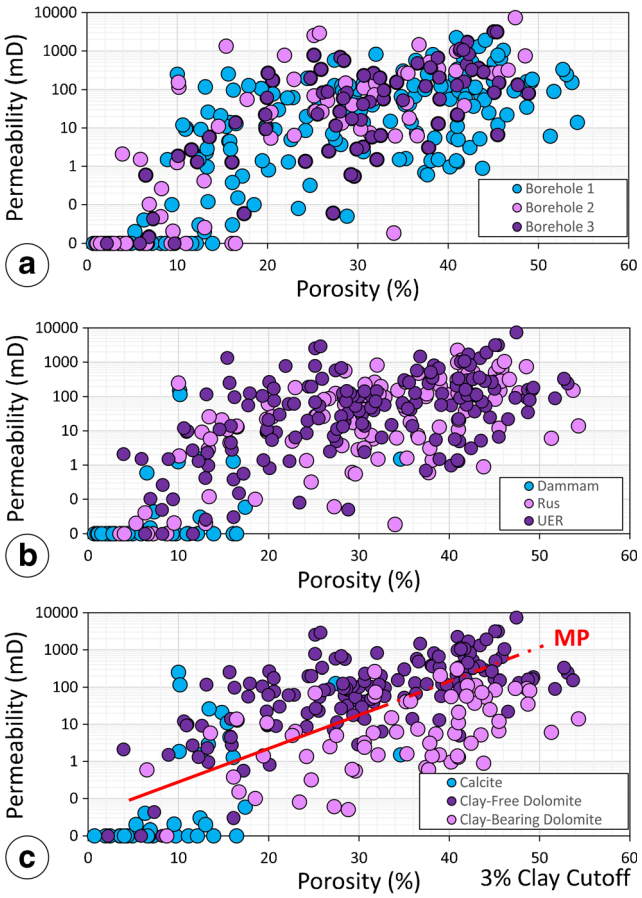

Fig. 21 Porosity-permeability plots for 2-in. plugs taken at ~0.75 m intervals for all cores ($n = 256$) where rock competency allowed. **a** Measurements delineated by borehole. **b** Measurements delineated by formation. **c** Measurements delineated by dominant mineralogy (low-Mg calcite vs dolomite) and by the presence of clay in dolomitized rocks (clay content greater than 3% based on XRD). The red line (MP) represents the global microporosity trend for limestones from Fullmer et al. (2014) and Kaczmarek et al. (2015)

faults were active in the Eocene, and linked to the topographic high separating the basins. The presence of such a reactivating fault systems was also concluded by Abu-Zeid (1991).

Bearing this model in mind, some additional observations in the three boreholes may be explained. First, in the Traina Member of the Rus Formation, the rocks of boreholes 2 and 3 are largely dolomites with only minor secondary clay minerals, whereas bedded clay deposits are observed in the Traina Member of borehole 1 (Figs. 5, 6, and 7). The implication is that the source of the clay-rich detritus to the south, perhaps reflecting the presence of low-gradient rivers at the margins of the restricted southern basin. Deposits of the overlying Al Khor Member are clay-bearing in all boreholes, indicating that the southern restricted basin had filled accommodation by that point, and clay-rich near-shore deposits (muddy tidal flats) could prograde across northern Qatar from the south. That stated, the best-developed and thickest tidal flat facies of the three boreholes are observed in the Al Khor Member of borehole 2. The Al Khor Member in boreholes 1 and 3 displays greater percentages of subtidal deposits. Therefore, the borehole 2 area may have remained a subtle high during late Rus Formation time. Rus Formation deposits in eastern Saudi Arabia contain "green shale" (Powers et al. 1966), perhaps indicating the siliciclastic source is associated with the Red Sea uplift.

It is interesting to note that open-marine facies are observed throughout the Dammam Formation at all locations. In spite of this, at least two intra-formational karstified surfaces have been recognized. The first is above the Rujm Aid Member (Fig. 18b), and the second is above the Midra Shale Member (Fig. 18d). To the north (borehole 3), these members, along with the Alveolina Member, all of which are assumed to have been widely deposited given their depositional facies, were apparently eroded prior to the deposition of the Umm Bab Member. These observations point toward repeated cycles of meteoric exposure with related karstification and erosion, and significant marine re-inundation during the Middle Eocene. The eustatic sea-level curve for the time interval of the Dammam Formation would not seem to vary enough to explain this pattern (Al-Saad 2005). It is therefore considered likely that regional or local tectonic uplift and subsidence, presumably associated with early Zagros formation, was an important control on both depositional settings and post-depositional removal of the Middle Eocene rock record of Qatar, with increased erosion focused to the north. Understanding the links between the Zagros uplift, with its associated forebulge dynamics, and the nature and thickness of the Cenozoic deposits of Qatar is a subject ripe for future research, with potential to significantly aid understanding of carbonate deposits formed in similar foreland basins of the ancient past.

Finally, based on the observations discussed above, and assuming the N-S cross-sectional line shown on Fig. 1a, conceptual (not to scale) tectono-stratigraphic model for Cenozoic rocks of Qatar can be offered (Fig. 23a, b). The model assumes the presence of a foreland basin to the north, associated with early Zagros uplift (Marzouk and El Sattar 1994; Glennie et al. 1990) and a fault-bounded platform interior basin to the south (Fig. 22a) (Tai et al. 2016). The model begins with time step 1 (Fig. 23a), deposition of informal Member C of the UER Formation in the Early Eocene, with Members A and B (Boukhary et al.

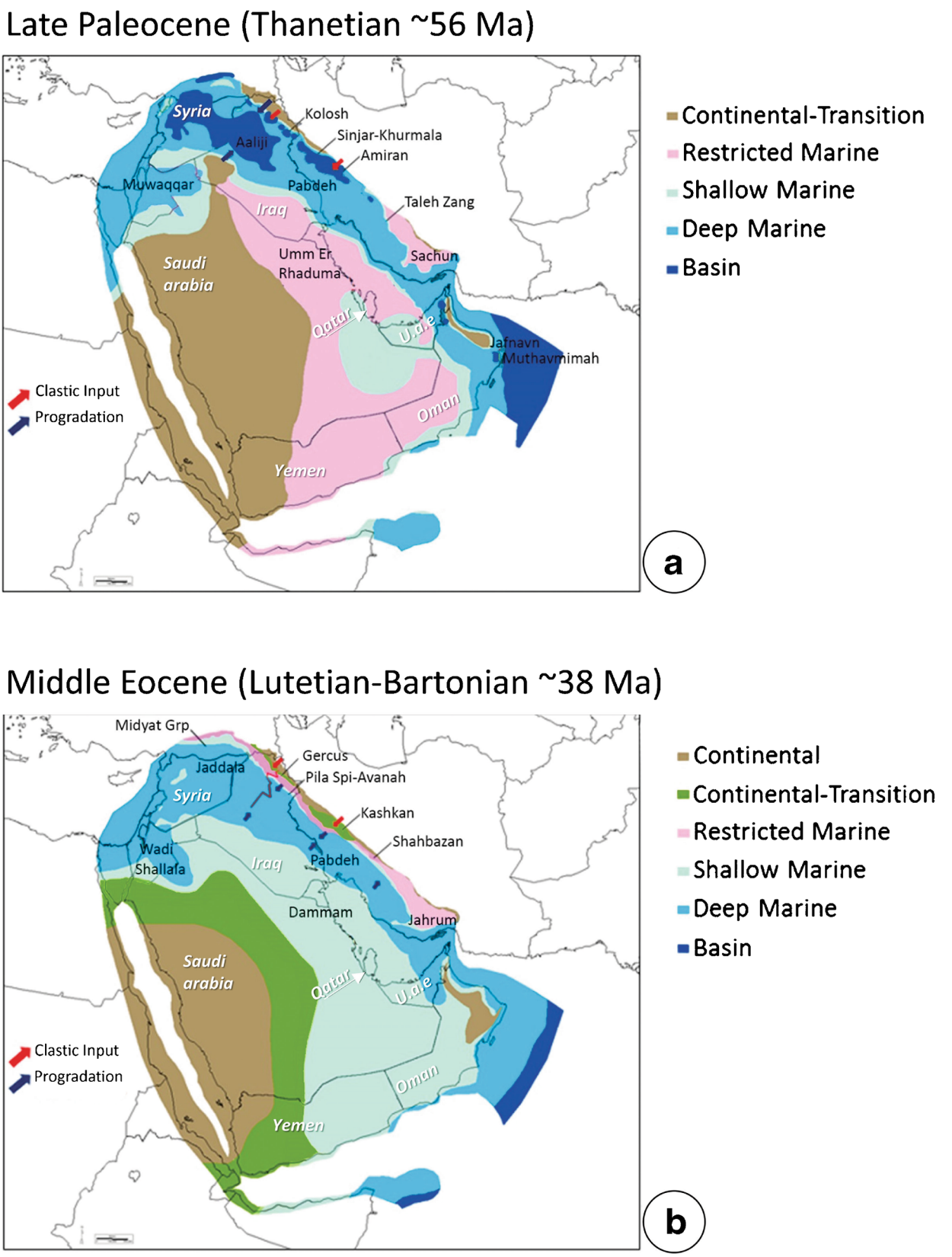

Fig. 22 Paleomaps showing depositional environments of the Arabian plate during **a** the Late Paleocene and **b** the Middle Eocene (Tai et al. 2016). During deposition of the of the UER Formation and Rus Formation, a separate and more restricted basin developed in southern Qatar, as well as eastern Saudi Arabian and in the United Arab Emirates

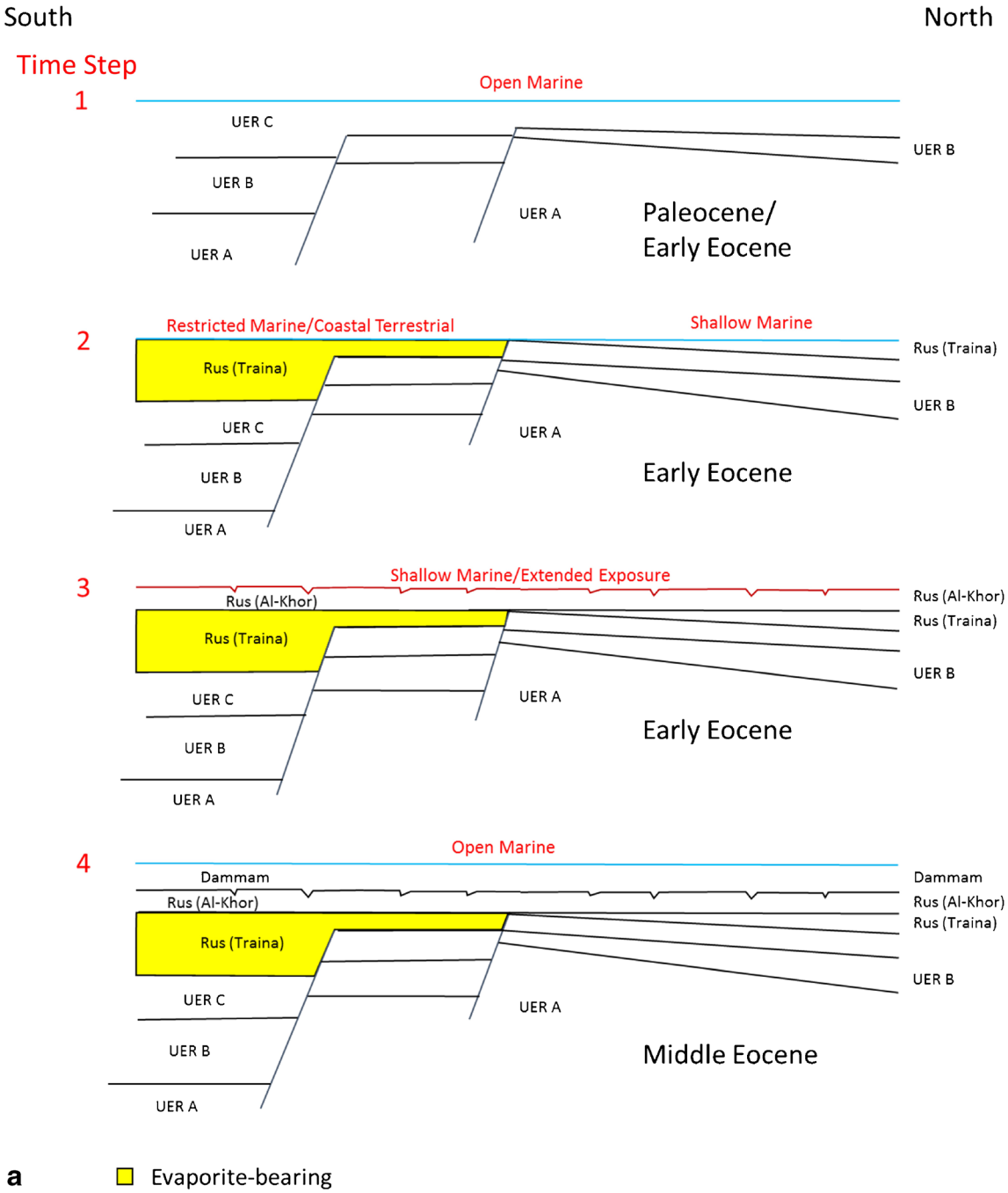

Fig. 23 **a** Tectono-stratigraphic model for Cenozoic rocks of Qatar based on regional and core-based observations, time steps 1–4 (see text). **b** Tectono-stratigraphic model for Cenozoic rocks for Qatar based on regional and core-based observations, time steps 5–7 (see text)

2011) shown underlying. Although the paleontological evidence is limited in the UER Formation of borehole 2, what is available (Fig. 13a) indicates open marine conditions in the elevated area between the basins. Therefore, the basins are assumed to be connected at this time. Time step 2 (Fig. 23a) shows the deposition of the Rus Formation, Traina Member, with separation between the northern and southern basins, at least during low-stands, and the formation of bedded gypsum deposits to the south and less-restricted shallow subtidal deposits to the north. During time step 3 (Fig. 23a), deposition of the Al Khor Member occurred. The southern basin accommodation was filled, and shallow subtidal and tidal-flat environments with land-derived clays migrated across Qatar from the south. Extended exposure occurred both during and at the end of Al Khor Member deposition. Significant transgressions occurred during the deposition of

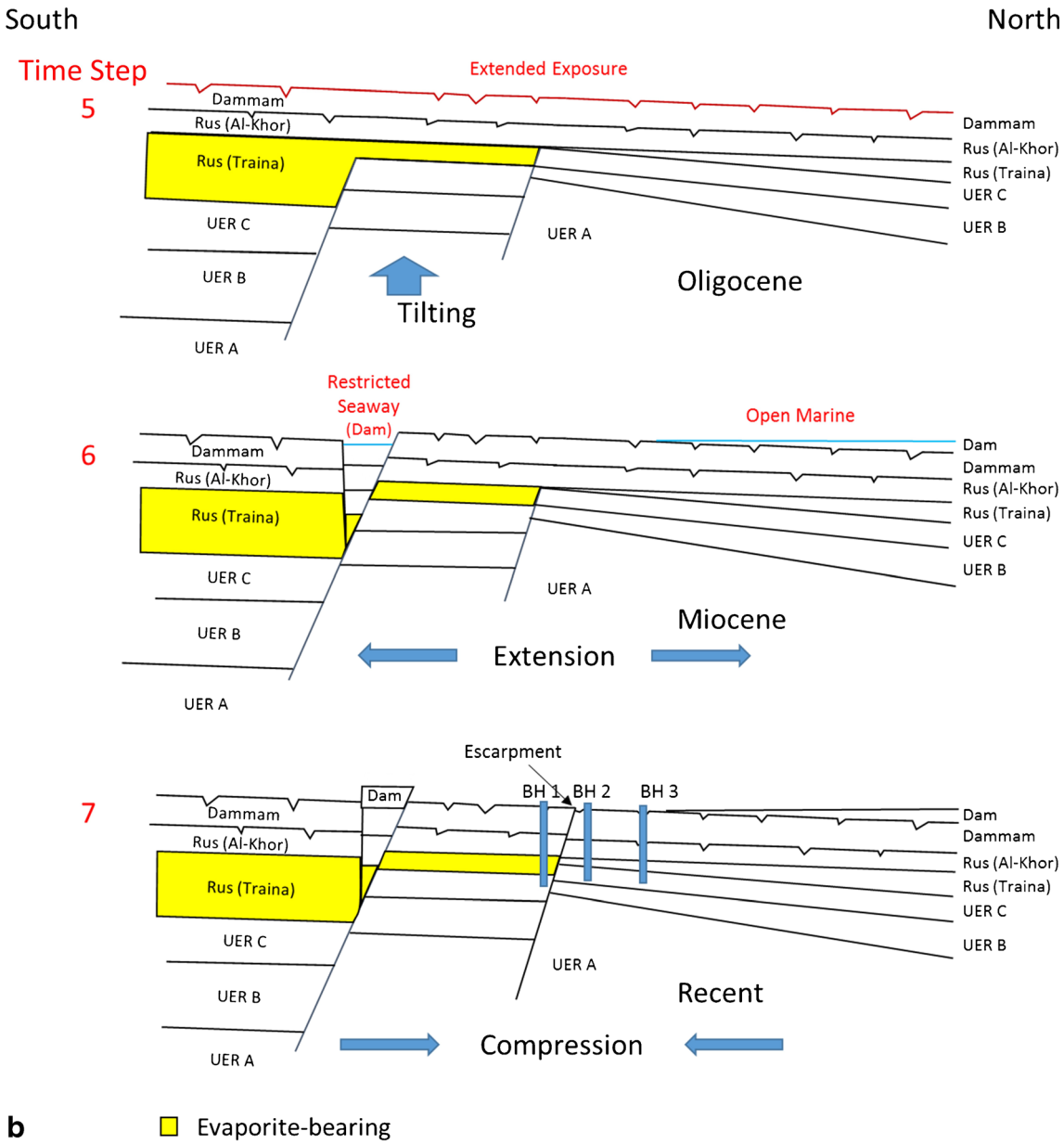

Fig. 23 (continued)

Dammam Formation (time step 4; Fig.23a) with open marine settings widespread across Qatar. Such inundations were interrupted by periods of exposure and karstification, likely related to tectonic uplift. Time step 5 (Fig. 23b) depicts the regional tilting associated with late Oligocene flexure (Van Buchem et al. 2014). This was a long period of exposure and karstification. During time step 6 (Fig. 23b), Miocene-age extension occurred, likely reactivating faults along the margin of the southern Eocene basin (Rivers and Larson 2018). Restricted marine deposits formed in narrow seaways (Dill et al. 2005) that opened in southwestern Qatar (Dam Formation). Offshore, North of Qatar, Dam Formation deposits unconformably onlap the underlying Dammam Formation (Van Buchem et al. 2014) and likely represent open marine deposits in the Zagros foreland basin at that time. Finally (time step 7; Fig.23b), recent compression has resulted in throw-reversal of Eocene-age basin-bounding faults, the uplift of the restricted Dam Formation, as well as the overlying Hofuf Formation (Rivers and Larson 2018), and formation of the central Qatar escarpment (Fig. 1).

Conclusions

Paleogene-age rocks of the Umm er Radhuma, Rus, and Dammam Formations form the near-surface aquifer rocks of Qatar. Rocks of the Umm er Radhuma Formation and the Rus Formation (Traina Member) were deposited in northern and southern basinal areas, separated by a fault-controlled

topographic high located in central Qatar. The southern basin was affected by input of fine siliciclastic sediment during deposition of the Rus Formation, Traina Member (Ypresian Stage), and was more restricted, resulting in gypsum precipitation from seawater concentrated by evaporation. At the same time, more normal marine depositional settings formed to the north, and carbonate deposits predominated. During deposition of the Al Khor Member of the Rus formation (Ypresian Stage), and of the Dammam Formation in general (Lutetian to Priabonian Stages), the basins were apparently connected, with restricted (Rus Formation) to open marine (Dammam Formation) deposition occurring across Qatar. Following extended Oligocene exposure, faults active during deposition of the Eocene strata were likely reactivated, both creating accommodation for Miocene deposits to the south (Dam Formation) and causing their subsequent uplift. Such structural reactivation also resulted in the formation of a prominent "V"-shaped escarpment in central Qatar. The connectivity, flow, and storage characteristics of Qatar near-surface aquifer rocks are in large part a function of their mineralogical makeup, the variability of which can be explained in context of sequence stratigraphic concepts and understanding of structural history.

Acknowledgments The authors would like to thank Tim Demko, Penny Patterson, Kevin Bohacs, Toni Simo, and Patrick Lehmann for their helpful suggestions. We are appreciative of Benjamin Rendall, Jacques Leblanc, and two anonymous reviewers for their insightful reviews. We thank Kahramaa and the Qatar Ministry of Municipality and Environment for permitting core recovery and the Qatar Center for GIS for providing mapping data.

References

Abdel-Fattah ZA, Kora MA, Ayyad SN (2013) Facies architecture and depositional development of Middle Miocene carbonate strata at Siwa Oasis, Northwestern Egypt. Facies 59:505–528

Abu-Zeid M (1991) Lithostratigraphy and framework of sedimentation of the subsurface Paleogene succession in northern Qatar. Arabian Gulf N Jb Geol Paliaiont Mh 4:191–204

Abu-Zeid M, Boukhary M (1984) Stratigraphy, facies and environment of sedimentation of the Eocene rocks in the Fhaihil (Gebel Dukhan) section, Qatar, Arabian Gulf. Rev Paléobiol 3:159–173

Al-Saad H (2003) Facies analysis, cyclic sedimentation and paleoenvironment of the Middle Eocene Rus Formation in Qatar and adjoining areas. Carbonates Evaporites 18:41–50

Al-Saad H (2005) Lithostratigraphy of the Middle Eocene Dammam Formation in Qatar, Arabian Gulf: effects of sea-level fluctuations along a tidal environment. J Asian Earth Sci 25:781–789

Al-Saad H, Ibrahim MI (2002) Stratigraphy, micropaleontology, and paleoecology of the Miocene Dam Formation, Qatar. GeoArabia 7:9–28

Baalousha HM (2016) Groundwater vulnerability mapping of Qatar aquifers. J Afr Earth Sci 124:75–93

Boukhary M, Alsharhan A (1998) A stratigraphic lacuna within the Eocene of Qatar: an example of the interior platform of the Arabian Peninsula. Rev Paléobiol 17:49–68

Boukhary M, Hewaidy AG, Luterbacher H, Bassiouni ME, Al-Hitmi H (2011) Foraminifera and ostracods of early Eocene Umm er Radhuma Formation, Dukhan oil field, Qatar. Micropaleontology 57:37–60

Cavalier C (1975) Le Tertiaire du Qatar en affleurement. Lexique Strat Int 3:89–120

Cavelier C, Salatt A, Heuze Y (1970) Geological description of the Qatar Peninsula (Arabian Gulf): explanation of the 1/100.000 geological map of Qatar. Bureau de Recherches Géologiques et Minières

Dill HG, Nasir S, Al-Saad H (2003) Lithological and structural evolution of the northern sector of Dukhan anticline, Qatar, during the early Tertiary: with special reference to sequence stratigraphic bounding surfaces. GeoArabia 8:201–226

Dill HG, Botz R, Berner Z, Stüben D, Nasir S, Al-Saad H (2005) Sedimentary facies, mineralogy, and geochemistry of the sulphate-bearing Miocene Dam Formation in Qatar. Sediment Geol 174:63–96

Dunham RJ (1962) Classification of carbonate rocks according to depositional textures. In: Ham WE (ed) Classification of carbonate rocks. AAPG Memoir 1:108–121

Ebanks W, Bubb JN (1975) Holocene carbonate sedimentation, Matecumbe Keys Tidal Bank, South Florida. J Sediment Petrography 45:422–439

Eccleston B, Pike J, Harhash I (1981) The water resources of Qatar and their development. vol I-III. Ministry of Industry and Agriculture Doha

Esteban M, Klappa CF (1983) Subaerial exposure environments. In: Scholle, P.A., Bebout, D.G., Moore, C.H. (eds.). Carbonate depositional environments. American Association Petroleum Geologists Memoir, 33:1–96

Fleitmann D, Matter A, Pint JJ, Al-Shanti MA (2004) The speleothem record of climate change in Saudi Arabia. Saudi Geological Survey, Jeddah, Kingdom of Saudi Arabia

Fullmer SM et al (2014) Microporosity: characterization, distribution, and influence on oil recovery. In: IPTC 2014: International Petroleum Technology Conference

Gao G, Land LS (1991) Nodular chert from the Arbuckle Group, Slick Hills, SW Oklahoma: a combined field, petrographic and isotopic study. Sedimentology 38:857–870

Geel T (2000) Recognition of stratigraphic sequences in carbonate platform and slope deposits: empirical models based on microfacies analysis of Palaeogene deposits in southeastern Spain. Palaeogeogr Palaeoclimatol Palaeoecol 55:211–238

Glennie K, Clarke MH, Boeuf M, Pilaar W, Reinhardt B (1990) Interrelationship of Makran-Oman Mountains belts of convergence. In: Robertson AHF, Searle MP, Ries AC (eds) The geology and tectonics of the Oman region, The geological society, vol 49. Special Publications, London, pp 773–786

Holail HM, Shaaban MN, Mansour AS, Rifai RI (2005) Diagenesis of the Middle Eocene Upper Dammam Subformation, Qatar: petrographic and isotopic evidence. Carbonates Evaporites 20:72–81

International Atomic Energy Agency (1992) Statistical treatment of data on environmental isotopes in precipitation. Technical Reports Series, 331. International Atomic Energy Agency

James N, Choquette PW (1990) Limestones—seafloor diagenetic environments. In: McIlreath IA, Morrow W (eds) Diagenesis. Reprint Series 4. Geoscience Canada, pp 13–34

Kabanov P, Anadón P, Krumbein WE (2008) Microcodium: an extensive review and a proposed non-rhizogenic biologically induced origin for its formation. Sediment Geol 205:79–99

Kaczmarek SE, Fullmer SM, Hasiuk FJ (2015) A universal classification scheme for the microcrystals that host limestone microporosity. J Sediment Res 85:1197–1212

Knauth LP, Epstein S (1976) Hydrogen and oxygen isotope ratios in nodular and bedded cherts. Geochim Cosmochim Acta 40:1095–1108

Seltrust Engineering Limited (1980) Qatar geological map, scale I: 100, 000 and explanatory booklet. Industrial Development Technical Center, Qatar

Marzouk I, El Sattar M (1994) Wrench tectonics in Abu Dhabi, United Arab Emirates. In: Al-Husseini MI (ed) Middle East Petroleum Geosciences, vol 1. GeoArabia, pp 655–668

Nasir SJ, Al-Saad H, Al-Sayigh AR, Al-Harthy AR, Almishwat A, Dill H (2003) Ferricretes of the Early Tertiary Dammam Formation in the Dukhan Area, Western Qatar: mineralogy, geochemistry, and environment of deposition. Qatar University Sci J 23:59–75

Pettke T, Halliday AN, Rea DK (2002) Cenozoic evolution of Asian climate and sources of Pacific seawater Pb and Nd derived from eolian dust of sediment core LL44-GPC3. Paleoceanography 17:1031

Powers R, Ramirez L, Redmond C, Elberg Jr. E 1966. Geology of the Arabian Peninsula: sedimentary geology of Saudi Arabia. US Geological Survey Professional Papers 560-D, 147 p

Pratt BR, James NP (1986) The St George Group (Lower Ordovician) of western Newfoundland: tidal flat island model for carbonate sedimentation in shallow epeiric seas. Sedimentology 33:313–343

Purser BH (1973) The Persian Gulf: Holocene carbonate sedimentation and diagenesis in a shallow epicontinental sea. Springer, Berlin Heidelberg

Retallack GJ (2001) Soils of the past: an introduction to paleopedology, 2nd edn. Blackwell Science Ltd, London

Rivers JM, Larson KP (2018) The Cenozoic kinematics of Qatar: evidence for high-angle faulting along the Dukhan 'anticline'. Mar Pet Geol 92:953–961

Saller AH (1984) Petrologic and geochemical constraints on the origin of subsurface dolomite, Enewetak Atoll: an example of dolomitization by normal seawater. Geology 12:217–220

Sarkar S (2017) Microfacies analysis of larger benthic foraminifera-dominated Middle Eocene carbonates: a palaeoenvironmental case study from Meghalaya, NE India (Eastern Tethys). Arab J Geosci 10:121

Seltrust Engineering Limited (1980) Qatar Geological Map, Scale I: 100, 000 and Explanatory Booklet. Industrial Development Technical Center, Qatar: 20

Sharland, PR, Archer R, Casey DM, Davies RB, Hall SH, Heward AP, Horbury, AD, Simmons, MD (2001) Arabian Plate sequence stratigraphy: GeoArabia Special Publication 2, Gulf PetroLink, Bahrain, 371 p

Shinn EA (1983) Tidal flat environment. In: Scholle PA, Bebout DG, Moore CH (eds) Carbonate depositional environments. American Association of Petroleum Geologists Tulsa, Oklahoma, USA

Strohmenger CJ, Jameson J (2014) Modern coastal systems of Qatar as analogues for arid climate carbonate reservoirs: improving geological and reservoir modelling. First Break 33:41–50

Tai PC, Grabowski GJ, Czernuszenko M, Liu C (2016) Cenozoic depositional history of the northeastern Arabian Plate, GEO2016 Bahrain

Van Buchem F, Svendsen N, Hoch E, Pedersen-Tatalovic R, Habib K (2014) Depositional history and petroleum habitat of Qatar. In: Marlow L, Kendall CCG, Yose LA (eds) Petroleum systems of the Tethyan region, Memoir 106. AAPG, pp 641-678

Van Gorsel J (1988) Biostratigraphy in Indonesia: methods, pitfalls and new directions. In: Indonesian Petroleum Association, Seventeenth Annual Convention, Jakarta, October 1988

Van Wagoner JC, Posamentier HW, Mitchum PR, Vail RM, Sarg JF, Loutit TS, Hardenbol J (1988) An overview of the fundamentals of sequence stratigraphy and key definitions. In Wilgus CK, Hastings BS, Kendall CGC, Posamentier HW, Ross CA, Van Wagoner JC (eds) Sea-level changes: an integrated approach. Society of Economic Paleontologists and Mineralogists Special Publication no. 42, pp 39–45

Warren JK (2016) Evaporites: a geological compendium. 2 edn. Springer International Publishing

Zamagni J, Mutti M, Košir A (2008) Evolution of shallow benthic communities during the Late Paleocene–earliest Eocene transition in the Northern Tethys (SW Slovenia). Facies 54:25–43